Recurrent De Novo and Biallelic Variation of *ATAD3A*, Encoding a Mitochondrial Membrane Protein, Results in Distinct Neurological Syndromes

Tamar Harel,[1,31,*] Wan Hee Yoon,[2,3,31] Caterina Garone,[4] Shen Gu,[1] Zeynep Coban-Akdemir,[1] Mohammad K. Eldomery,[1] Jennifer E. Posey,[1] Shalini N. Jhangiani,[1,5] Jill A. Rosenfeld,[1,6] Megan T. Cho,[7] Stephanie Fox,[8] Marjorie Withers,[1] Stephanie M. Brooks,[9] Theodore Chiang,[5] Lita Duraine,[2,3] Serkan Erdin,[10,11] Bo Yuan,[1,6] Yunru Shao,[1] Elie Moussallem,[1] Costanza Lamperti,[12] Maria A. Donati,[13] Joshua D. Smith,[14] Heather M. McLaughlin,[7] Christine M. Eng,[1,6] Magdalena Walkiewicz,[1,6] Fan Xia,[1,6] Tommaso Pippucci,[15] Pamela Magini,[16] Marco Seri,[15,16] Massimo Zeviani,[12] Michio Hirano,[17] Jill V. Hunter,[18] Myriam Srour,[19] Stefano Zanigni,[20,21] Richard Alan Lewis,[1,22,23] Donna M. Muzny,[5] Timothy E. Lotze,[23,24] Eric Boerwinkle,[5,25] Baylor-Hopkins Center for Mendelian Genomics, University of Washington Center for Mendelian Genomics, Richard A. Gibbs,[1,5] Scott E. Hickey,[9] Brett H. Graham,[1] Yaping Yang,[1,6] Daniela Buhas,[8,26] Donna M. Martin,[27,28] Lorraine Potocki,[1,23] Claudio Graziano,[15] Hugo J. Bellen,[1,2,3,29,30] and James R. Lupski[1,5,22,23,*]

ATPase family AAA-domain containing protein 3A (ATAD3A) is a nuclear-encoded mitochondrial membrane protein implicated in mitochondrial dynamics, nucleoid organization, protein translation, cell growth, and cholesterol metabolism. We identified a recurrent de novo *ATAD3A* c.1582C>T (p.Arg528Trp) variant by whole-exome sequencing (WES) in five unrelated individuals with a core phenotype of global developmental delay, hypotonia, optic atrophy, axonal neuropathy, and hypertrophic cardiomyopathy. We also describe two families with biallelic variants in *ATAD3A*, including a homozygous variant in two siblings, and biallelic *ATAD3A* deletions mediated by nonallelic homologous recombination (NAHR) between *ATAD3A* and gene family members *ATAD3B* and *ATAD3C*. Tissue-specific overexpression of bor^{R534W}, the *Drosophila* mutation homologous to the human c.1582C>T (p.Arg528Trp) variant, resulted in a dramatic decrease in mitochondrial content, aberrant mitochondrial morphology, and increased autophagy. Homozygous null *bor* larvae showed a significant decrease of mitochondria, while overexpression of bor^{WT} resulted in larger, elongated mitochondria. Finally, fibroblasts of an affected individual exhibited increased mitophagy. We conclude that the p.Arg528Trp variant functions through a dominant-negative mechanism that results in small mitochondria that trigger mitophagy, resulting in a reduction in mitochondrial content. *ATAD3A* variation represents an additional link between mitochondrial dynamics and recognizable neurological syndromes, as seen with *MFN2*, *OPA1*, *DNM1L*, and *STAT2* mutations.

Introduction

Remodeling of the mitochondrial membrane through continuous cycles of fusion and fission promotes mixing of mitochondrial proteins and DNA, ensuring proper function.[1–3] Pathogenic variation in genes encoding fusion and fission factors, including *MFN2* (MIM: 608507),[4–7] *OPA1* (MIM: 605290),[8,9] *DNM1L* (MIM: 603850),[10,11] *STAT2* (MIM: 600556),[12] *SLC25A46* (MIM: 610826),[13] and *GDAP1* (MIM: 606598)[14] have been associated with

[1]Department of Molecular and Human Genetics, Baylor College of Medicine, Houston, TX 77030, USA; [2]Department of Molecular and Human Genetics, Jan and Dan Duncan Neurological Research Institute, Baylor College of Medicine, Houston, TX 77030, USA; [3]Howard Hughes Medical Institute, Jan and Dan Duncan Neurological Research Institute, Baylor College of Medicine, Houston, TX 77030, USA; [4]MRC Mitochondrial Biology Unit, Cambridge CB2 OXY, UK; [5]Human Genome Sequencing Center, Baylor College of Medicine, Houston, TX 77030, USA; [6]Baylor Genetics, Baylor College of Medicine, Houston, TX 77030, USA; [7]GeneDx, Gaithersburg, MD 20877, USA; [8]Medical Genetics Department, Montreal Children's Hospital, Montreal, QC H4A 3J1, Canada; [9]Department of Pediatrics, The Ohio State University College of Medicine, Division of Molecular and Human Genetics, Nationwide Children's Hospital, Columbus, OH 43205, USA; [10]Center for Human Genetic Research, Massachusetts General Hospital, Boston, MA 02114, USA; [11]Program in Medical and Population Genetics, Broad Institute of MIT and Harvard, Cambridge, MA 02142, USA; [12]Unit of Molecular Neurogenetics, The Foundation "Carlo Besta" Institute of Neurology-IRCCS, Milan 20126, Italy; [13]Metabolic and Muscular Unit, Meyer Children's Hospital, University of Florence, Florence 50132, Italy; [14]Department of Genome Sciences, University of Washington, Seattle, WA 98195, USA; [15]Medical Genetics Unit, Policlinico Sant'Orsola-Malpighi, University of Bologna, Bologna 40138, Italy; [16]Medical Genetics Unit, Department of Medical and Surgical Science, University of Bologna, Bologna 40138, Italy; [17]Department of Neurology, Columbia University Medical Center, New York, NY 10032, USA; [18]Department of Pediatric Radiology, Texas Children's Hospital, Houston, TX 77030, USA; [19]Department of Pediatrics, Neurology and Neurosurgery, McGill University, Montreal, QC H4A 3J1, Canada; [20]Functional MR Unit, Policlinico S. Orsola - Malpighi, Bologna 40138, Italy; [21]Department of Biomedical and Neuromotor Sciences (DIBINEM), University of Bologna, Bologna 40123, Italy; [22]Department of Pediatrics, Baylor College of Medicine, Houston, TX 77030, USA; [23]Texas Children's Hospital, Houston, TX 77030, USA; [24]Department of Pediatric Neurology, Texas Children's Hospital, Houston, TX 77030, USA; [25]Human Genetics Center, The University of Texas Health Science Center, Houston, TX 77030, USA; [26]Human Genetics Department, McGill University, Montreal, QC H3A 0G4, Canada; [27]Department of Pediatrics and Communicable Diseases, University of Michigan, Ann Arbor, MI, 48109; [28]Department of Human Genetics, University of Michigan, Ann Arbor, MI 48109, USA; [29]Program in Developmental Biology, Jan and Dan Duncan Neurological Research Institute, Baylor College of Medicine, Houston, TX 77030, USA; [30]Department of Neuroscience, Jan and Dan Duncan Neurological Research Institute, Baylor College of Medicine, Houston, TX 77030, USA
[31]These authors contributed equally to this work
*Correspondence: harel.tamar@gmail.com (T.H.), jlupski@bcm.edu (J.R.L.)
http://dx.doi.org/10.1016/j.ajhg.2016.08.007.

recognizable human syndromes including optic atrophy, peripheral neuropathy, cardiomyopathy, brain malformations, and developmental delay as recurrent features.

ATAD3A (MIM: 612316) is ubiquitously expressed and encodes an ATPase family AAA-domain containing protein 3A (ATAD3A) that simultaneously interacts with the outer and inner mitochondrial membranes. In vitro studies show that ATAD3A is involved in diverse cellular processes, including mitochondrial dynamics,[15] mitochondrial DNA (mtDNA) maintenance and replication,[16] channeling of cholesterol for steroidogenesis,[17,18] and resistance of cancer cells to therapy.[19,20] Co-immunoprecipitation in lung adenocarcinoma cell lines revealed evidence for interaction of ATAD3A with MFN2, OPA1, and DNM1L,[21] suggesting that ATAD3A may affect mitochondrial dynamics via interaction with these proteins.

The ATAD3 gene family in humans includes three paralogs (*ATAD3A*, *ATAD3B* [MIM: 612317], and *ATAD3C*) positioned in tandem on chromosome 1p36.33 and appears to have recently evolved by duplication of a single ancestral gene.[22,23] Disruption of the *Drosophila* ortholog (*bor*), which has ~70% similarity to human *ATAD3A*, results in growth arrest during larval development.[15] The ortholog in *C. elegans* is essential for mitochondrial activity and development.[24] *Atad3* homozygous null mice are embryonic lethal at day E7.5 due to growth retardation and defective development of the trophoblast lineage, whereas heterozygotes for a loss-of-function allele seem unaffected.[22] RNAi studies of ATAD3A in HeLa and lung cancer cells have documented increased mitochondrial fragmentation and a decreased co-localization of mitochondria and endoplasmic reticulum (ER).[21] Despite multiple studies in vitro and in animal models, the precise function of ATAD3A has not been elucidated to date.

We identified an identical de novo heterozygous variant in *ATAD3A* in five individuals. In addition, we identified two families with biallelic single-nucleotide variants (SNVs) or copy-number variants (CNVs) involving *ATAD3A*. Our data indicate that both monoallelic and biallelic pathogenic variation in *ATAD3A* led to the observed neurological phenotypes in these seven families. Functional studies in fibroblasts from an affected individual and in *D. melanogaster* revealed significant mitochondrial abnormalities and indicate that ATAD3A is required to maintain the proper size and number of mitochondria in neurons and muscles.

Material and Methods

Subjects

Families 1, 2, 3, 5, and 7 provided consent according to the Baylor-Hopkins Center for Mendelian Genomics (BHCMG) research protocol H-29697, approved by the Institutional Review Board (IRB) at Baylor College of Medicine (BCM). Families 4 and 6 provided consent according to protocol M0010, approved by the IRB at Meyer Children Hospital, Florence, and protocol 13084, approved by the IRB at AUSL, Bologna, respectively. Subjects are described further in Tables 1 and S1.

Whole-Exome Sequencing

Family 1, II-2 (proband), family 5 (parents and proband), and family 7 (proband) had whole-exome sequencing (WES) at Baylor Genetics (BG, BCM) according to the protocol described in Yang et al.[25] After clinical WES results were unrevealing for a potential etiologic molecular diagnosis in known disease genes, parental exome sequencing for family 1 was obtained through the BHCMG research initiative. In brief, DNA samples were prepared into Illumina paired-end libraries and underwent whole-exome capture with the BCM-HGSC core design (52 Mb, Roche NimbleGen), followed by sequencing on the Illumina HiSeq 2000 platform (Illumina). Data produced were aligned and mapped to the human genome reference sequence (hg19) by the Mercury pipeline.[26] Single-nucleotide variants (SNVs) were called with the ATLAS (an integrative variant analysis pipeline optimized for variant discovery) variant calling method and annotated by the in-house-developed "Cassandra" annotation pipeline that uses ANNOVAR (Annotation of Genetic Variants) and additional tools and databases.[27–29] De novo variants were calculated by an in-house developed pipeline (DNM-Finder) for in silico subtraction of parental variants from the proband's variants in vcf files while accounting for the read number information extracted from BAM files. Bioinformatic tools predicted conservation and pathogenicity of candidate variants, and variants were compared against both an internal database (~5,000 exomes) and publicly available databases such as the 1000 Genomes Project, the Exome variant server, NHLBI GO Exome Sequencing Project (ESP), the Atherosclerosis Risk in Communities Study (ARIC) Database, and the Exome Aggregation Consortium (ExAC) database. Families 5 and 7 were identified through an internal database. The GeneMatcher tool facilitated identification of four additional families with variants of interest in *ATAD3A*.[30] Detailed sequencing methods for these families can be found in the Supplemental Data.

PCR Amplification and Sanger Sequencing

An amplicon containing the *ATAD3A* variant was amplified from genomic DNA by conventional PCR, with a primer design that ensured specific amplification of *ATAD3A* and not its homolog *ATAD3B*. Representative primers for family 1, II-2 were ATAD3A-F1 (5′-CCC CTC CAA AGA GGA TGT TT-3′) and ATAD3A-R1 (5′-CAA CTG AGC ATC TCC ACA GC-3′). Additionally, the homologous exon of *ATAD3B* was sequenced with a specific intronic primer: ATAD3B-F1 (5′-TGC CTC ACT TGG GAA CTC C-3′) and ATAD3B-R1 (5′-ACA GAA GCT CCC ACA TGA CA-3′). PCR products were purified by ExoSAP-IT (Affymetrix) and analyzed by standard Sanger di-deoxy nucleotide sequencing (DNA Sequencing Core Facility, Baylor College of Medicine). Details for Sanger validation and segregation of variants in other individuals can be found in the Supplemental Data.

3D Modeling of Protein Structure

The 3D protein structure model of ATAD3A (GenBank: NM_001170535.1) was predicted by I-TASSER.[31,32] The side chain orientation of the mutant residue was obtained by the PyMol Molecular Graphics System, v.1.5 Schrodinger, LLC. Amino acid conservation was obtained from the Consurf server based on sequence analysis.[33]

Biochemistry

The activities of mitochondrial respiratory chain complexes (I-IV) and Citrate Synthase (CS) were measured in skeletal muscle

Table 1. Comparison of the Phenotypic Features of Seven Individuals with *ATAD3A* Variants

	Monoallelic					Biallelic		
	Family 1, II-2	**Family 2, II-4**	**Family 3, II-1**	**Family 4, II-1**	**Family 5, II-1**	**Family 6, II-1**	**Family 6, II-2**	**Family 7, II-1**
Age at last exam	9 years	5 years	3 years	5 years	23 months	26 years	24 years	5 days
Gender	F	F	M	F	M	F	M	F
DD	+	+	+	+	+	+	+	NR
ID	+ (mild)	+	+	+	+	+ (mild)	−	NR
Seizures	−	−	−	−	−	+	+	+
Optic atrophy	+	−	+	+	−	−	−	−
Congenital cataract	−	−	−	−	−	+	+	−
Corneal clouding	−	−	−	−	−	−	−	+
Hypotonia	+	+	+	+	+	+	+	+
Spasticity	+	+	+	+	−	−	−	+
Pectus carinatum	−	−	+	−	−	−	+	−
Peripheral neuropathy	+	+	+	+	borderline	−	−	NR
Hypertrophic cardiomyopathy	−	−	+	+	−	−	−	mild RVH with septal hypertrophy (newborn)
Elevated plasma lactate	−	+ (mild)	+ (intermittent)	+	NR	NR	+	NR
Cerebellar atrophy/ hypoplasia	−	−	−	−	−	+ (moderate)	+ (mild)	+ (severe)
MR spectroscopy	normal	NR	lactate peak	NR	NR	reduction of left cerebellar hemisphere NAA	normal	reduction of NAA, increased choline
Other	ADHD	deficiency complex I+III	methyl-glutaconic aciduria; growth hormone deficiency; dystonia	methyl-glutaconic aciduria; deficiency complex II+III, II+CS	47,XXY	delayed puberty, hyposomia	delayed puberty, delayed bone age, hyposomia, cryptorchidism	smooth sulcal/gyral pattern, hypoplasia of posterior fossa structures, intubated at birth; deceased at 13 days

Abbreviations are as follows: ADHD, attention deficit hyperactivity disorder; CS, citrate synthase; DD, developmental delay; F, female; ID, intellectual disability; IQ, intelligence quotient; M, male; MR, magnetic resonance; NAA, N-acetyl aspartate; NR, not reported; RVH, right ventricular hypertrophy.

homogenates and digitonin-treated cultured skin fibroblasts as described previously.[34] Activities are expressed relative to CS for the muscle or relative to mitochondrial protein for fibroblasts.

Detection of CNV from WES Read Depth Analysis

Internal databases were screened for homozygous CNVs using two in-house-developed algorithms. The first method utilized a dual normalization approach consisting of principal component analysis (PCA)-XHMM[35] intermediates and read per kilobase per million mapped reads (RPKM). The former normalized raw read depth values with PCA, which were then centered by exon target on a Z-score scale, whereas the latter was normalized at the sample level (RPKM). The intersection of two orthogonal normalization approaches (target based and sample based) allowed for an enhancement in signal and reduction in noise. In each method, we removed exons with extreme GC content and low complexity biases from analysis. Regions with either very high or very low GC content are more likely to be captured poorly by WES. Complete homozygous and hemizygous exon deletions were called by strict filtering criteria, including exon target Z-scores less than −2 and RPKM equal or near 0. The second algorithm, in the R programming language, was also based on the total number of reads (TR) in each exon and normalized read depth values (RPKM).

High-Density Array Comparative Genomic Hybridization

To further characterize the CNVs involving the *ATAD3A* genomic region, we designed an 8× 60K oligonucleotide array with ~200 bp per probe spacing from Agilent Technologies (AMADID 082882). DNA from HapMap individual NA15510 was used as hybridization control. Scanned array images were processed using Agilent Feature Extraction software (v.10) and extracted files were analyzed using Agilent Genomic Workbench (v.7.0.4.0). Array designs and sequence alignment for breakpoint analysis were based on the February 2009 genome build (GRCh37/hg19 assembly).

Evaluation of CNV Boundaries and Breakpoint Junction Analysis

Droplet digital PCR (ddPCR) was performed using the QX200 AutoDG Droplet Digital PCR System from Bio-Rad according to manufacturer's protocols. In brief, a 20 μL mixture was set up for each PCR reaction, containing 10 μL of 2× Q200 ddPCR EvaGreen Supermix, 0.25 μL of each primer (10 μM) and 20 ng of genomic DNA. Reaction mixture was subjected to automatic droplet generation, followed by PCR reaction and droplet reading. Cycling conditions for PCR were as follows: 5 min at 95°C, 40 cycles of 30 s at 95°C/1 min at 67.1°C/1 min at 72°C, 5 min at 4°C, 5 min at 90°C and final hold at 4°C. Ramp rate was set for 2°C per s for all steps. Data were analyzed with QuantaSoft Software (Bio-Rad), and concentrations of positive droplets (number of positive droplets per μL of reaction) were obtained for each PCR reaction. Raw data of ddPCR and primer sequences are shown as Table S2.

The breakpoint junctions were amplified with either TaKaRa LA Taq (Clontech) or QIAGEN HotStarTaq DNA Polymerase according to the manufacturer's protocol. The breakpoint junction of BAB8733 (family 7, II-2) was amplified with the following primers: BAB8733_del_F1 (5′-TTG GAG TTC TGT GGT CCT GG-3′) and BAB8733_del_R1 (5′-CAG GCC CAC ACT GCT GAC-3′), while the wild-type allele was amplified with BAB8733_wt_F2 (5′-ATG GGC ACA GTC ACA GGT TT-3′) and BAB8733_del_R1. The breakpoint junction of BAB8734 (family 7, II-1) was amplified with the primers BAB8734_del_F3 (5′-GAG AGC GGA GTC CAC ACC-3′) and BAB8734_del_R3 (5′-GGA AAC CAA CCA CAC ACG G-3′), while the wild-type allele was amplified with BAB8734_del_F3 and BAB8734_wt_R4 (5′-CTG ATC CAC CGA CAG AAG CAG-3′).

Miropeats

The Miropeats program descriptively illustrates the genomic architecture by plotting the intra-species alignments of the reference genome. ICAass (v.2.5) algorithm performed DNA sequence comparisons, and Miropeats (v.2.01) was then applied for converting the comparisons into graphical display based on the position and matching quality.[36] A threshold of 200 was set for comparison of human paralogs.

Fly Strains and Maintenance

The following stocks were obtained from the Bloomington Stock Center at Indiana University (BDSC):

w^{1118}*; PBac{PB}bor*^{c05496}*/TM6B, Tb*^{1}

w^{1118}*; Df(3R)Exel7329/TM6B, Tb*^{1}[37]

y^{1} w*; tubulin-Gal4/*TM3, Sb*^{1} *Ser*^{1}

w*; *Ubi-Gal4 /CyO*

yw;+; n-syb-Gal4

w; D42-Gal4 UAS-mito-HA-GFP e/TM6B, Tb (from Bill Saxton)

w; *C57-Gal4*

All flies were maintained at room temperature (21°C). All crosses were kept at 21°C except those for *C57-Gal4* (25°C).

Cloning and Transgenesis

LD30988, an EST of *bor* (Drosophila Genomics Resource Center), contains a mutation that causes a substitution of an amino acid (D40 to Y) and an insertion of 72 additional nucleotides near the 3′ end. These mutations were corrected by site-directed PCR using primers bor Y40→D-F (5′-acg gcc ggc gag aag tcc ggg Gat tcg caa ctg agc cgg gcg-3′) and bor Y40→D-R (5′-cgc ccg gct cag ttg cga atC ccc gga ctt ctc gcc ggc cgt-3′); LD30988-F (5′-CAG CCT GCC GCT GCG GGT GCC AAG cgg ttc aaa ctg gac acc ttt gat-3′) and LD30988-R (5′-atc aaa ggt gtc cag ttt gaa ccg CTT GGC ACC CGC AGC GGC AGG CTG-3′). All final clones were confirmed by sequencing.

To generate *bor* p.Arg534Trp (R534W) (equivalent to human p.Arg528Trp), we performed site-directed mutagenesis using primers 5′-ctg tgc gag ggt atg tcg ggt TgG gaa atc tcc aag ctg ggc-3′ and 5′-gcc cag ctt gga gat ttc CcA acc cga cat acc ctc gca cag-3′. The corrected *bor* EST clone and *bor* (R534W) clone were amplified by PCR using primers bor-F BamHI (5′-cat ttt GGA TCC aaa ATG TCG TGG CTT TTG GGC AGG-3′) and bor-R NotI (5′-tgt aaG CGG CCG CTT ACA GTT TCT TTG CAG TTA G-3′). The PCR products were subcloned into BglII/NotI sites in a pUASTattB[38] vector to generate pUASTattB-bor^{WT} and pUASTattB-bor^{R534W}. The pUASTattB constructs were injected into *y,w,ΦC31; VK37* embryos[39] and transgenic flies were selected.

Larvae Dissection and Immunostaining

For muscle and axon staining, third instar larvae were dissected as described in Bellen and Budnik.[40] In brief, third instar larvae were fixed in 4% formaldehyde for 30 min at room temperature, rinsed in PBS twice, and washed in PBS containing 0.3% Triton X-100 three times. The primary antibodies were used at the following dilutions: mouse anti-ATP5A 1:500 (abcam), chick anti-GFP 1:1,000 (abcam), mouse anti-Dlg 1:250 (mAb 4F3, DSHB; developed by C.S.

Goodman, Renovis), and rabbit anti-HRP 1:1,000 (Jackson ImmunoResearch). Alexa 488-conjugated (Invitrogen) and Cy3- or Cy5-conjugated secondary antibodies (Jackson ImmunoResearch) were used at 1:120. Samples were mounted in Vectashield (Vector Labs). Alexa Fluor 568 phalloidin (ThermoFisher) was used at 1:1,000.

Bright-Field Imaging and Transmission Electron Microscopy of Flies

Drosophila larval muscles and neuro-muscular junctions (NMJs) were imaged according to standard electron microscopy procedures using a Ted Pella Bio Wave processing microwave with vacuum attachments. In brief, whole first instar larvae were dissected at room temperature under modified Karnovski's fixative consisting of 2% paraformaldehyde, 2.5% glutaraldehyde, in 0.1 M sodium cacodylate buffer at pH 7.2. The NMJ muscle samples were filleted under modified Karnovski's fixative and allowed to sit pinned under fixative for 40 min. After dissection the first instar larvae and NMJs were fixed for 2 days in fresh modified Karnovski's fixative rotating in a 4°C cold room. After 2 days in fixative, the samples were irradiated using the Ted Pella Biowave Microwave, rinsed three times with Millipore water, post-fixed with 1% aqueous Osmium Tetroxide, and rinsed again three times with Millipore water.

Concentrations from 30%–100% of ethanol were used for the initial dehydration series, followed with propylene oxide as the final dehydrant. The samples were gradually infiltrated with 3 ratios of propylene oxide and Embed 812, finally going into three changes of pure resin all under vacuum. Samples were allowed to infiltrate in pure resin overnight on a rotator. The samples were embedded into flat silicone molds and cured in the oven at 62°C for 3 days. The polymerized samples were thin-sectioned at 50 nm and stained with 1% uranyl acetate for 12 min followed by lead citrate for 2 min before TEM examination. Grids were viewed in a JEOL 1400 Plus transmission electron microscope at 80 kV. Micrographs were captured by an AMT XR-16 mid-mount 16 mega-pixel digital camera.

Fibroblast Culture and TEM

Human fibroblasts were grown in DMEM (10569-010, Life Technologies) supplemented with 10% fetal bovine serum (FBS) and penicillin-streptomycin (Sigma) at 37°C. For fixation, cells were placed in a 50:50 media/fix solution with Karnovski's fixative (2% paraformaldehyde and 2.5% glutaraldehyde in 1% sodium cacodylate buffer) for 10 min, followed by 100% Karnovski's fixative for 45 min. Cells were scraped and placed into micro-centrifuge tubes, spun down at 1,500 × *g* for 3 min, and left in fresh fixative for 15 min after an additional centrifugation. The cell pellets were then subjected to a normal processing procedure as above.

Immunoblotting Analysis

Protein concentration was quantitated using the Bio-Rad DC protein assay. 10 μg of total lysate or DDM-treated crude mitochondria protein were analyzed by electrophoresis in NuPage Novex 4%–12% bis-tris gel (Invitrogen). After electrophoresis, proteins were transferred electrophoretically to a PVDF membrane and probed with the following antibodies: rabbit polyclonal anti-ATAD3A (1:1,000, Novus Biological), anti-GAPDH (1:10,000, Abcam), or anti-VDAC1 (1:10,000, Abcam). HRP-conjugated anti-rabbit or anti-mouse IgG secondary antibodies (Promega) were used at a dilution of 1:3,000. The protein bands were visualized by chemiluminescence, using reagents purchased from GE Healthcare.

Results

De Novo *ATAD3A* Variant Is Associated with Optic Atrophy and Peripheral Neuropathy

The clinical findings of five affected individuals from five families with an identical, recurrent de novo variant in *ATAD3A* (g.chr1:1464679C>T [hg19]; GenBank: NM_001170535.1; c.1582C>T [p.Arg528Trp], Figures 1 and S1–S4) are summarized in Tables 1 and S1; detailed case reports can be found in the Supplemental Data and photographs are available in Figure 2. The phenotypic spectrum included developmental delay (5/5), hypotonia (5/5), optic atrophy (3/5), peripheral neuropathy (4/5), and hypertrophic cardiomyopathy (2/5). Mitochondrial dysfunction was suggested in different cases by intermittently or mildly elevated plasma lactate, a lactate peak on MR spectroscopy, slightly increased excretion of 3-methylglutaconic acid, and/or deficiency in respiratory chain activities on muscle homogenate (Supplemental Data). These phenotypic features bear striking resemblance to those encountered with pathogenic variation in other mitochondrial fission and fusion proteins, including *DNM1L*,[10,11] *MFN2*,[5,7] *OPA1*,[8,9] and *SLC25A46*[13] (Figure S5).

The c.1582C>T variant has robust bioinformatic damaging predictions (Table S3), arose at a CpG dinucleotide (Figure 1B),[41–43] and was absent from internal and publicly available databases, including the ExAC database of ~60,000 unrelated individuals. 3D structural modeling further supported pathogenicity, as the long side chain of arginine at position 528 is replaced by the flat aromatic ring of tryptophan and alters the configuration of a conserved pocket, possibly a functional site (Figure 1D). To ensure that the variant was specific to *ATAD3A* and to investigate the possibility of gene conversion from the highly homologous *ATAD3B*, primer design was targeted to specific intronic sequences flanking the exon. No variation was seen in *ATAD3B*, suggesting that the c.1582C>T variant is specific to *ATAD3A*. This argues against gene conversion as a mutational mechanism (Figure S1).

Sanger sequencing of the maternal sample in family 4 suggested low-level mosaicism in genomic DNA derived from blood (Figure S3). Nerve conduction velocities of the mother (family 4, I-2) were within normal range; however, she had cardiac arrhythmia diagnosed in childhood and required a pacemaker, which might be a clinical phenotype relevant to the *ATAD3A* variation given the cardiac phenotype in two individuals with the recurrent de novo variant and our inability to assess the degree of mosaicism in the mother's heart tissue. The proband in family 5 had a dual molecular diagnosis, including Klinefelter syndrome and the *ATAD3A* variant. Dual molecular diagnoses have been documented in ~4.6%–7.2% of molecularly diagnosed individuals.[25,44–46] Both of these clinical situations, parental mosaicism and dual molecular diagnoses, require specific consideration with respect to prognosis and recurrence risk for the families.[47,48]

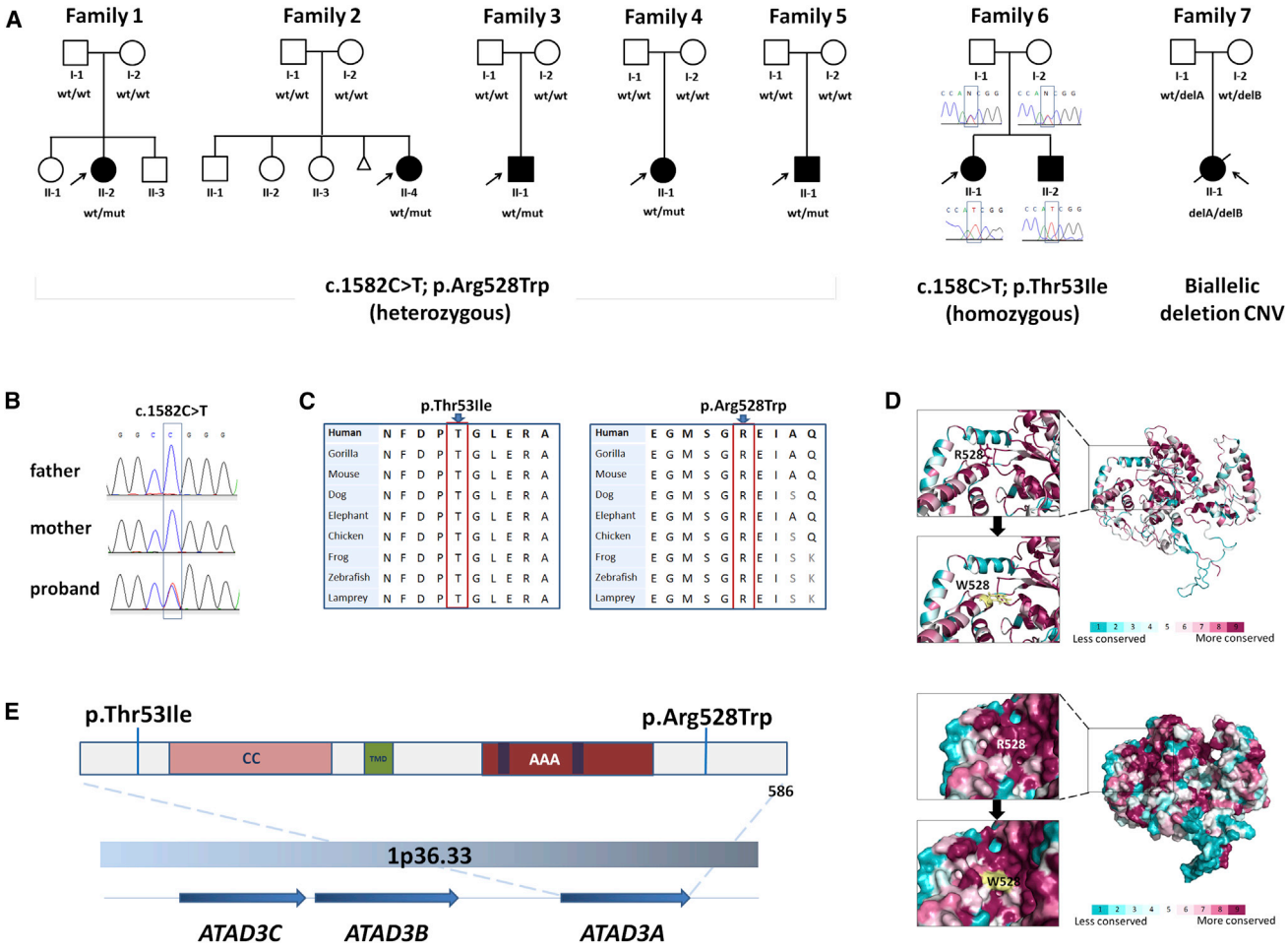

Figure 1. Pedigrees and *ATAD3A* Variant Details
(A) Pedigrees of studied families, indicating the recurrent de novo single-nucleotide variant (SNV) in *ATAD3A* in families 1–5, a homozygous SNV in family 6, and compound heterozygous deletion copy-number variants (CNVs) in family 7.
(B) Sanger validation of the *ATAD3A* variant in family 1.
(C) The p.Thr53Ile and p.Arg528Trp substitutions alter conserved residues.
(D) Protein structure prediction shows replacement of the arginine long side chain by a flat aromatic ring of tryptophan. Color spectrum indicates high conservation of the Arg528 residue. Surface structure modeling indicates that the arginine at position 528 resides in a conserved pocket, possibly a functional site. The mutation alters the configuration of the pocket.
(E) Schematic representation of ATAD3A (isoform 2) with indication of the coiled-coil domain (CC), transmembrane domain (TMD), and AAA domain including Walker A and Walker B ATP-binding and ATPase domains, respectively. Localization of the altered residues in families 1–6 is indicated. The three human ATAD3 genes are located in tandem on chromosome 1p36.33.

Homozygous *ATAD3A* Single-Nucleotide Variant Identified in Siblings with Congenital Cataract, Ataxia, and Seizures

In a sixth family (Figures 1A and 2I–2L), two siblings born to distantly related parents presented with motor developmental delay, speech delay, congenital cataracts, seizures, ataxia, hypotonia, and reduced muscle strength in the extremities (Tables 1, S1, Supplemental Data). Magnetic resonance imaging (MRI) revealed hypoplasia of the optic nerves and cerebellar atrophy (Figures 2O and S6), and magnetic resonance spectroscopy (MRS) revealed a moderate reduction of N-acetyl aspartate to creatine (NAA/Cr) ratio in the cerebellum, indicating neuronal-axonal degeneration. No CSF lactate was detected. Muscle biopsy of the male sibling showed slight increase of Oil Red O (ORO) and sub-sarcolemmal COX activities. Mitochondrial respiratory chain enzyme analysis in muscle homogenate and in skin fibroblasts revealed normal activities (Table S4). The variant with the strongest bioinformatic predictions shared by the siblings was a homozygous *ATAD3A* variant (g.chr1:1447806C>T [hg19]; GenBank: NM_001170535.1; c.158C>T [p.Thr53Ile]), found in an ~700 kb run of homozygosity (ROH). Bioinformatic predictions and in silico modeling supported pathogenicity (Table S3, Figure S7). The genetic data suggest that biallelic variation in *ATAD3A* might lead to a distinct neurological phenotype as a recessive disease trait.

Biallelic Deletion of *ATAD3A* Is Associated with Infantile Lethality

The high homology between the three *ATAD3* paralogs, as depicted by Miropeats alignment of this region to itself

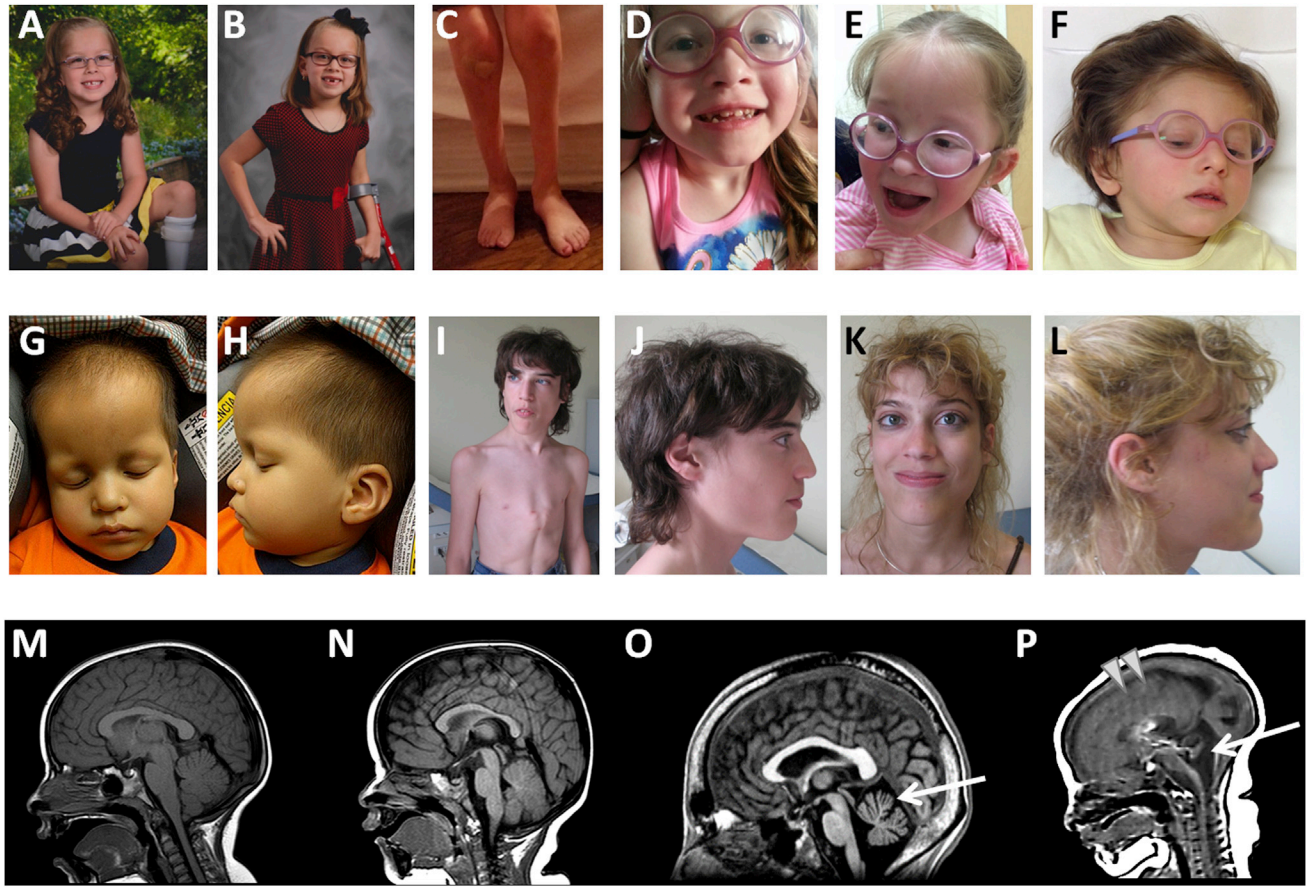

Figure 2. Clinical Findings of Affected Individuals
(A–C) Family 1, II-2 at 6 years (A) and 8 years (B), showing high forehead (B) and marked atrophy of the lower legs (C).
(D and E) Family 2, II-4 at 5 years with high forehead, small nose, and thin hair.
(F) Family 4, II-1 at 5 years with triangular facies, micrognathia, and low-set ears.
(G and H) Family 5, II-1 at 23 months, with frontal bossing, deep set eyes, and micrognathia.
(I–L) Individuals II-2 (I, J) and II-1 (K, L) from family 6, demonstrating elongated face, triangular nose and prognathism, and pectus carinatum (I).
(M–P) Mid-sagittal T1-weighted brain magnetic resonance imaging (MRI) images from affected individuals.
(M and N) Individuals with heterozygous recurrent de novo variant show either no significant abnormalities (M, family 1, II-2 at 6 years) or prominent extra-axial spaces and incomplete myelination (N, family 5, II-1 at 8 months).
(O) Family 6, II-1, harboring a homozygous *ATAD3A* missense variant, had moderate atrophy of the cerebellum (arrow) at age 26 years.
(P) MRI of family 7, II-1, with biallelic deletion of *ATAD3A*, showed very poor gyration and sulcation (arrowheads) and hypoplastic cerebellum, vermis, and brainstem (arrow).

(Figure 3A), provides an endogenous genome architecture as substrate for nonallelic homologous recombination (NAHR) in this region and is predicted to make this locus susceptible to genomic instability.[49,50] Indeed, multiple heterozygous CNVs at the *ATAD3* locus have been reported in the Database of Genomic Variants (DGV, Figure S8A), yet no biallelic CNVs are reported.

Through analysis of WES data read depth, we identified a case subject with a biallelic deletion involving exons 1–5 of *ATAD3A* (Figure 3B). The proband (BAB8780 or family 7, II-1 in Figure 1A) had reduced fetal movement, respiratory failure requiring intubation at birth, cloudy corneas, seizures, and cerebellar and brainstem hypoplasia (Figure 2P). He died at 13 days. Targeted array comparative genomic hybridization (aCGH) (Figures S9A and S9B) and droplet digital PCR on parental samples (Figure 3C), followed by amplification of the breakpoint junctions (Figures 3D and 3E), revealed two distinct deletions. In the maternal sample (BAB8733), deletion of a ~38 kb segment was mediated by NAHR between the highly homologous fifth introns of *ATAD3B* and *ATAD3A* (Figure 4A). The approximate breakpoint junctions are located within chr1: 1,416,438–1,417,192 and 1,454,542–1,455,296 (hg19). Sanger sequencing showed a stretch of 754 bp with 100% identity at the breakpoint junctions, including an *Alu*Sx1 element (Figures S8B and S10A). In the paternal sample (BAB8734), deletion of a ~68 kb segment was mediated by NAHR between the highly homologous region spanning exons 7 and 11 in *ATAD3C* and *ATAD3A*, respectively (Figure 4). The approximate breakpoint junctions are located within chr1: 1,391,287–1,392,247 and chr1: 1,459,379–1,460,339 (hg19). Sanger sequencing revealed a stretch of

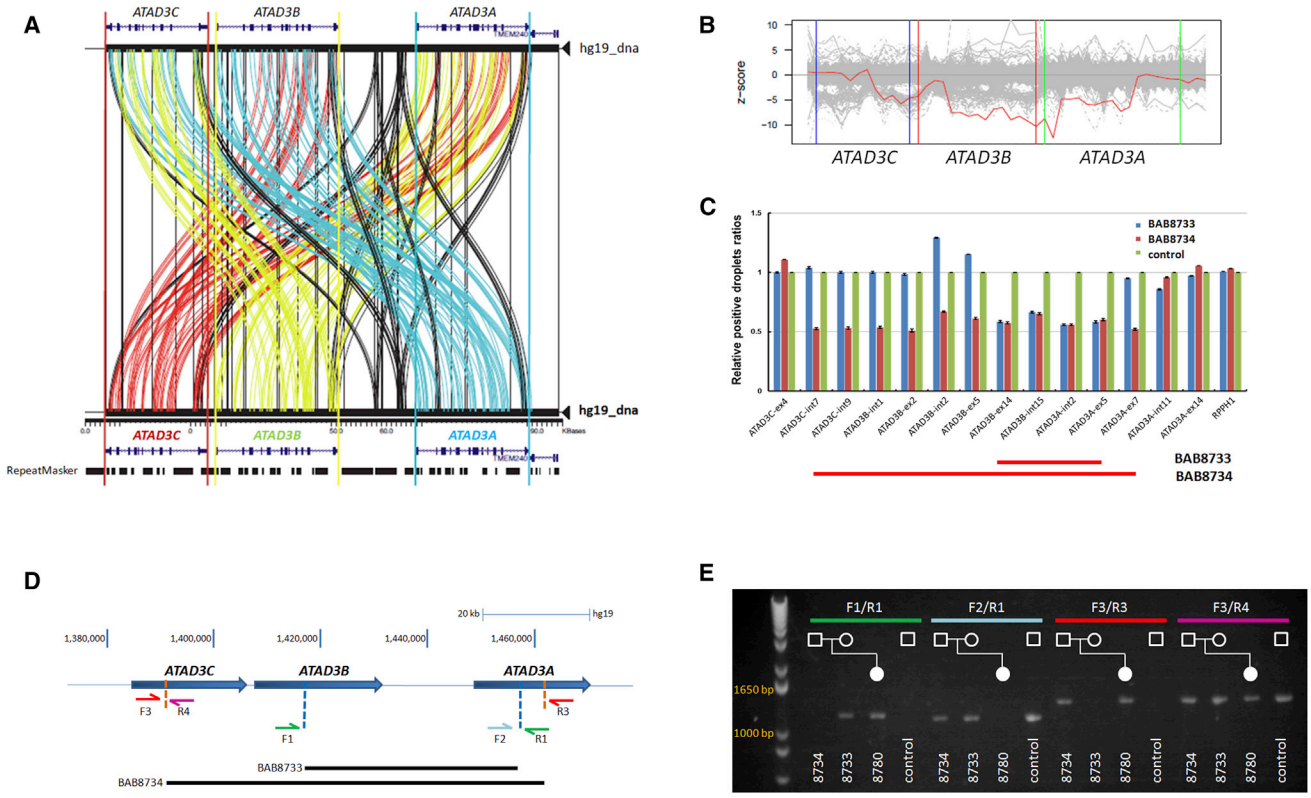

Figure 3. Compound Heterozygous Copy-Number Variation in Family 7

(A) Miropeats alignment of the *ATAD3* region indicates homology of the three *ATAD3* paralogs. *ATAD3C* reference sequence is indicated in red, *ATAD3B* reference sequence is indicated in green, and *ATAD3A* reference sequence is indicated in blue.

(B) Target Z score of PCA-normalized read depths for 44 exon targets of the three *ATAD3* genes. Comparative read depth data obtained from 2,634 WES samples are shown in gray (clinical collection). Family 7, II-1 is shown in red. Target Z score of PCA-normalized read depths for 16 exons (x axis) spanning portions of *ATAD3B* and *ATAD3A* have large negative Z scores (y axis), indicating a copy loss of both alleles.

(C) Droplet Digital PCR (ddPCR) detected a larger heterozygous deletion in BAB8734 (father) than the heterozygous deletion in BAB8733 (mother). Primer pairs targeting various exonic or intronic regions of *ATAD3C*, *ATAD3B*, and *ATAD3A* and a control primer pair targeting *RPPH1* were used to perform ddPCR in BAB8733 (mother), BAB8734 (father), and a control individual N/A10851. *RPPH1* is a gene known to have exactly two copies in the human genome. Ratios of concentrations of positive droplets were plotted for each amplicon tested against the control individual. For a region without deletion, the expected ratio is ~1, whereas for heterozygous deletion, the expected ratio is ~0.5 (one deleted copy-number versus two copies). Corresponding raw data of ddPCR and primer sequences are shown in Table S1.

(D) Schematic of primer design targeting maternal and paternal deletions and wild-type alleles. PCR amplicons indicating segregation of maternal deletion allele (F1/R1) and paternal deletion allele (F3/R3). Note that proband (BAB8780) lacks wild-type allele amplified by F2/R1 but does have wild-type allele amplified by F3/R4 since the latter is positioned outside the maternal deletion and can be amplified from this allele.

(E) Results of PCR breakpoint analysis. Proband inherited both the maternal and paternal deletions.

960 bp with 99.7% homology at the breakpoint junction and 273 bp with 100% identity (Figure S10B). The paternal deletion was not found in 100 population-matched white controls, as evaluated by breakpoint junction PCR (data not shown). The proband inherited both deletions (Figure 3E), presumably leading to loss of both functional copies of *ATAD3A*. A heterozygous deletion similar to that observed in the mother was identified previously in 1/15,767 individuals (dbVar: nsv545010),[51] and a heterozygous deletion similar to that of the father—spanning from *ATAD3C* to *ATAD3A*—was present in 13/873 (~1.5%) individuals (dbVAR: dgv2e212).[52] The latter frequency suggests that homozygous or compound heterozygous deletions of *ATAD3A* may be a source of morbidity in humans. This outcome may be under-recognized, perhaps due to genomic complexity at the locus, issues with the ability to uniquely map sequencing reads to the reference sequencing reads because of the presence of the gene family at this locus, poor coverage on some clinically available aCGH platforms, and small size of these intergenic deletion CNVs.

We also identified a subject (BAB761) with an apparent homozygous deletion of *ATAD3C* and *ATAD3B*, not involving *ATAD3A* and confirmed by aCGH and ddPCR (Figures S9C, S9D, and S11). BAB761 had previously been assigned a clinical and molecular diagnosis of Smith-Magenis syndrome (SMS [MIM: 182290]), associated with a second, heterozygous deletion on chromosome 17p11.2 encompassing *RAI1* (MIM: 607642).[53] Hence, we concluded that homozygous deletion of *ATAD3C* and *ATAD3B* does not have a substantial impact on phenotype and narrowed the critical region for the *ATAD3* locus to *ATAD3A*.

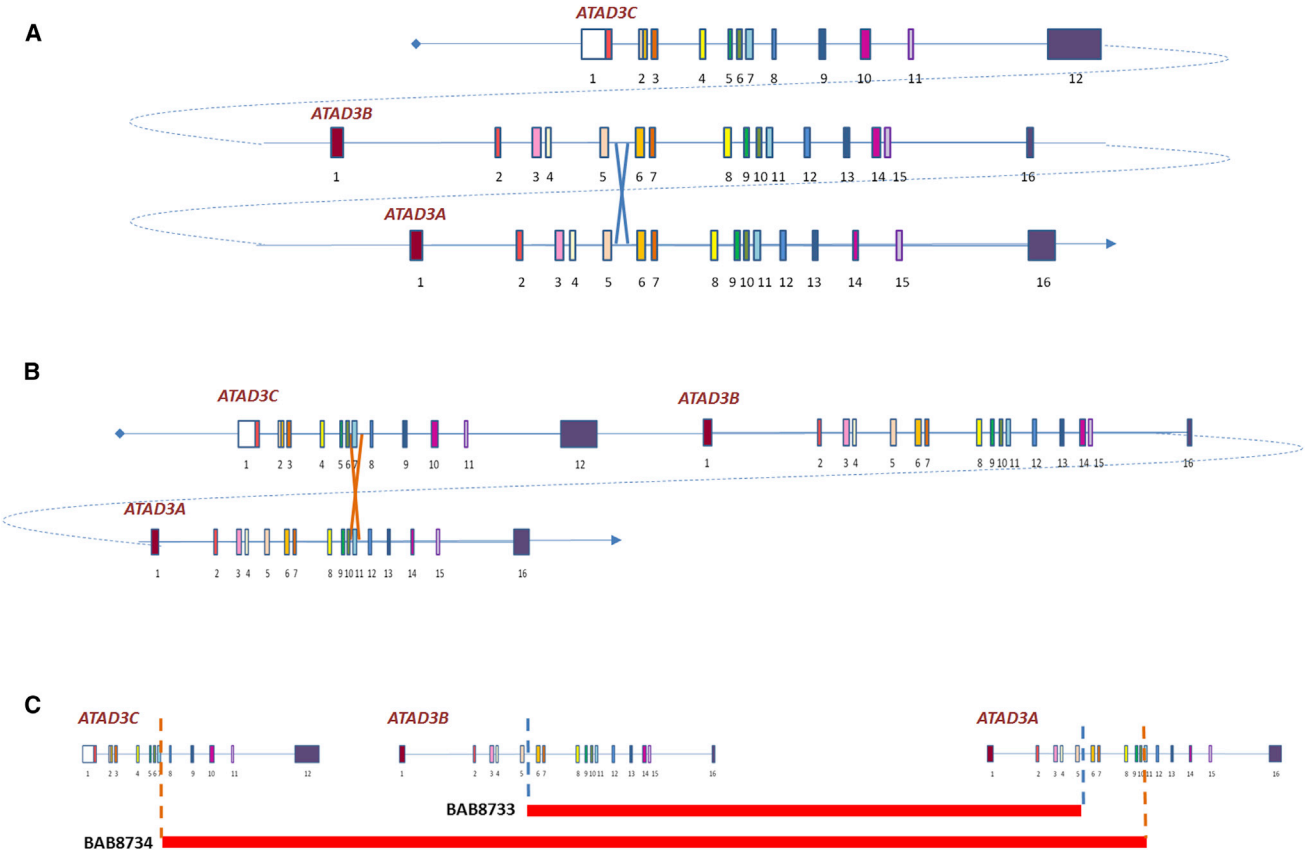

Figure 4. CNVs in Family 7 Are Mediated by NAHR
(A) Homologous exons of the three *ATAD3* genes are represented by similar colors. The deletion in BAB8733 (mother) is mediated by nonallelic homologous recombination (NAHR) between the fifth introns of *ATAD3B* and *ATAD3A*.
(B) The deletion in BAB8734 (father) is mediated by NAHR between the region of exon 7 of *ATAD3C* and exon 11 of *ATAD3A*.
(C) The boundaries of both deletions are represented by dotted lines.

The Fly p.Arg534Trp Variant Causes a Dramatic Loss of Mitochondria in Flies

To functionally evaluate the potential pathogenicity of the recurrent de novo p.Arg528Trp variant, we generated transgenic flies harboring a wild-type or variant UAS-cDNA copy (p.Arg534Trp, equivalent to human p.Arg528Trp) of *bor*, the fly homolog of *ATAD3A* (*UAS-bor*^{WT} and *UAS-bor*^{R534W}). This allowed us to drive these cDNA with tissue-specific Gal4 drivers. Ubiquitous expression of *bor*^{R534W} (*tub-* or *Ubi-Gal4 > UAS-bor*^{R534W}), as well as pan-neuronal (*n-syb-panneuronal-Gal4 > UAS-bor*^{R534W}) and motor neuron-specific (*D42-motorneurons-Gal4 > UAS-bor*^{R534W}) expression, all caused lethality, whereas *bor*^{WT} expression (*tub-*, *Ubi-Gal4, n-syb-panneuronal-Gal4,* or *D42-motorneurons-Gal4 > UAS-bor*^{WT}) did not affect viability or cause any other obvious phenotype (Figure 5A). Muscle-specific expression of *bor*^{R534W} (*C57-muscles-Gal4 > UAS- bor*^{R534W}) led to ~90% lethality (Figure 5A). Hence, *bor*^{R534W} expression causes dramatic reductions in survival when expressed in all neurons, motor neurons, or muscles, suggesting that the protein is highly toxic. It may therefore act as either a dominant-negative or a gain-of-function mutation.

At the cellular level, we noted that motor neurons expressing *bor*^{R534W} exhibited a dramatic reduction in mitochondria in cell bodies in the ventral nerve cord (VNC), axons, and synaptic boutons (Figures 5B–5E), suggesting that expression of the variant severely affects mitochondrial biogenesis[54] or mitochondrial dynamics, leading to mitophagy. When expressed specifically in larvae body wall muscles, the signal intensity of the mitochondrial marker ATP5A in *bor*^{R534W}-expressing muscles was significantly reduced when compared to *bor*^{WT}-expressing muscles or wild-type controls, consistent with our observation in motor neurons (Figures 6A and 6C). Transmission electron microscopy (TEM) revealed that muscles expressing *bor*^{R534W} contain very few small mitochondria with highly aberrant cristae (Figure 6B, arrowheads) and display a substantive increase in autophagic intermediates (Figure S12). In contrast, overexpression of *bor*^{WT} resulted in an increase in the number of large elongated mitochondria (Figures 6B and 6D). These data indicate that Bor^{WT} promotes fusion or inhibits fission, or affects both, whereas Bor^{R534W} inhibits fusion or promotes fission.

Fibroblasts from individual II-2 in family 1 at age 9 years showed a significant increase in mitophagy (Figures 6E, 6F, and S13) and a reduction, though not significant, in mitochondrial content (Figure S14). In conjunction with the fly data, this indicates that the p.Arg528Trp variant interferes

A

Gal4 drivers / Transgenes	tubulin-Gal4 (ubiquitous)	Ubi-Gal4 (Ubiquitous)	nsyb-Gal4 (neuron)	D42-Gal4 (motor neuron)	C57-Gal4 (muscle)
UAS-bor-wt	viable	viable	viable	viable	viable
UAS-bor (R534W)	lethal	lethal	lethal	lethal	viable

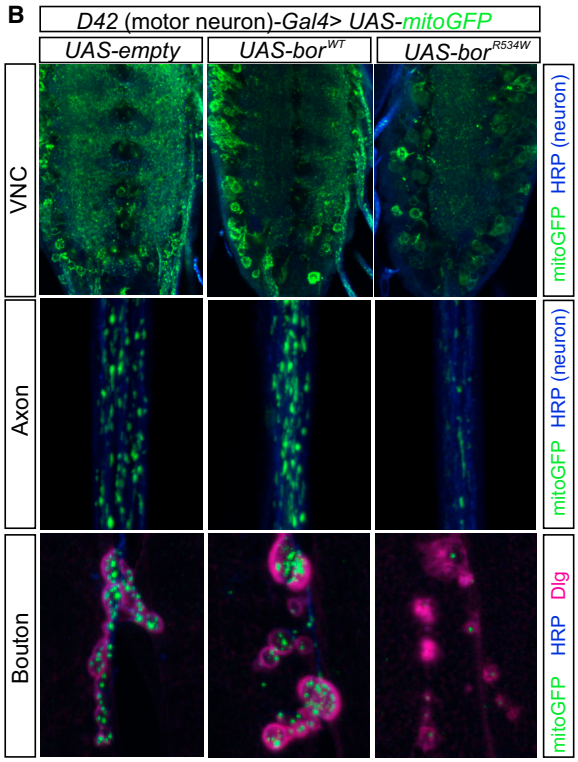

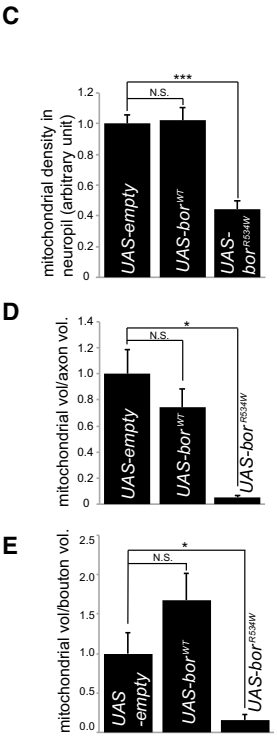

Figure 5. Expression of *Drosophila* ATAD3A Ortholog *bor* with p.Arg534Trp Leads to a Decrease in Mitochondria in Motor Neurons

(A) Effects of expression of wild-type *bor* and bor^{R534W}, driven by different *Gal4* drivers, on viability.

(B) Confocal micrographs of ventral nerve cord (VNC), axons, and boutons from third instar larvae carrying *D42-Gal4* and *UAS-mito-GFP* (green) together with *UAS-empty* (control), $UAS\text{-}bor^{WT}$, or $UAS\text{-}bor^{R534W}$. Neurons are labeled by HRP (blue) and boutons by Dlg (red).

(C) Quantification of mitochondrial density in VNC neuropil in control, $UAS\text{-}bor^{WT}$, or $UAS\text{-}bor^{R534W}$ larvae carrying *D42-Gal4*, *UAS-mito-GFP* together with the respective vectors.

(D and E) Quantification of mitochondrial volume in axons (D) and in boutons (E) of larvae carrying *D42-Gal4*, *UAS-mito-GFP* together with *UAS-empty*, $UAS\text{-}bor^{WT}$, or $UAS\text{-}bor^{R534W}$.

(C–E) Error bars indicate standard error of the mean (SEM). p values were calculated by Student's t test. *p < 0.05, ***p < 0.001. N.S. indicates not statistically significant.

with mitochondrial dynamics by either promoting fission or inhibiting fusion, which in turn may trigger mitophagy.

To assess the loss-of-function phenotypes associated with *bor*, we performed TEM on first instar larvae that lack *bor* just prior to their death and identified a dramatic decrease in mitochondrial content, similar to overexpression of Bor^{R534W} (Figures 6G and 6H). Given the similarities between the phenotypes associated with the loss of function of *bor* and the overexpression of bor^{R534W}, we propose that Bor^{R534W} acts as a strong dominant-negative mutation. This is supported by our finding that steady-state levels of ATAD3A protein in fibroblasts of the proband in family 4 are comparable to controls, when assayed both in total lysate and in crude mitochondria (Figure S15).

Discussion

We report eight individuals from seven families with monoallelic or biallelic variation involving both SNVs and CNVs at the *ATAD3A* locus, all presenting with a primarily neurologic disease. The clinical syndrome associated with the recurrent de novo c.1582C>G variant, observed in five families, manifests within a phenotypic and metabolic spectrum including global developmental delay, hypotonia, optic atrophy, axonal neuropathy, hypertrophic cardiomyopathy, lactic acidosis, and/or increased excretion of Krebs cycle intermediates. Several of these features overlap with phenotypes associated with other mitochondrial fission and fusion proteins (Figure S5), as exemplified by *DNM1L* (severe developmental delay, optic atrophy, peripheral neuropathy, lactic acidemia [MIM: 614388]),[10,11] *MFN2* (axonal peripheral neuropathy and variable optic atrophy [MIM: 609260]),[5,7] *OPA1* (optic atrophy, variable peripheral neuropathy,[8] and recently described hypertrophic cardiomyopathy [MIM: 165500 and 125250]),[9] and *SLC25A46* (axonal peripheral neuropathy and optic atrophy [MIM: 616505]).[13]

The recurrence of the de novo c.1582C>T variant in five distinct probands is likely attributable to a mutational hotspot at a CpG dinucleotide.[41–43] However, it is unclear from this initial study whether this is the only variant that can lead to a dominant phenotype, or if the bias is due to the CpG mutational hotspot. Three of the most highly mutable nucleotides known in the human genome are at CpG sites (*FGFR3* [MIM: 100800], *DMD* [MIM: 310200], and *FGFR2* [MIM: 101200]),[55] with two more recent examples (*KCNC1* [MIM: 616187][56] and *PACS1* [MIM: 607492]).[57]

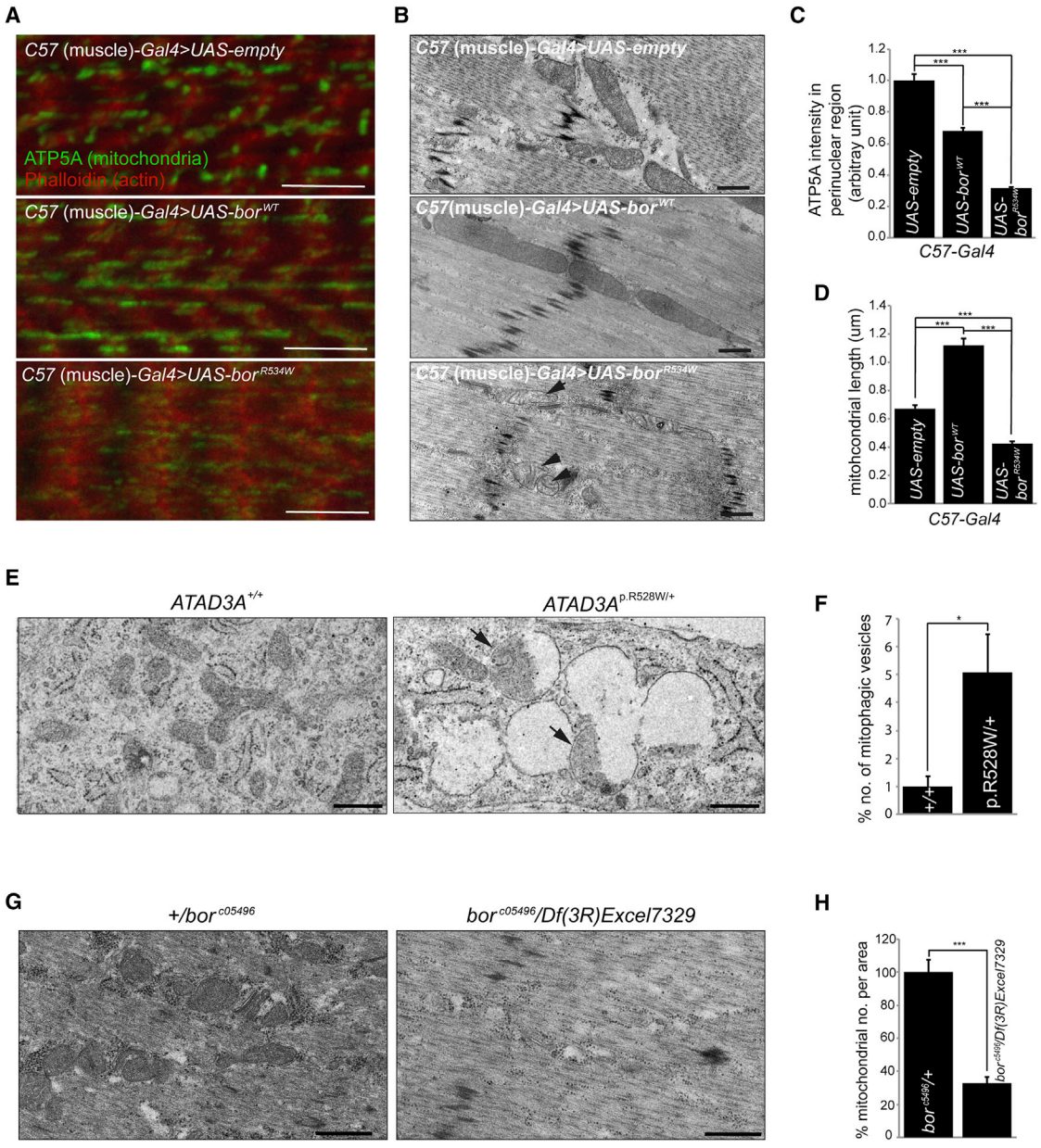

Figure 6. Expression of *Drosophila* ATAD3 Ortholog *bor* with p.Arg534Trp Variant in Muscle Causes a Decrease of Mitochondria

(A) Confocal micrographs of muscle from third instar larvae carrying *C57-Gal4* together with *UAS-empty* (control), *UAS-bor*^{WT}, or *UAS-bor*^{R534W}. ATP5A (green) labels mitochondria. Phalloidin (red) labels actin. Scale bars represent 10 μm.

(B) TEM of muscle from third instar larvae carrying *C57-Gal4* together with *UAS-empty* (control), *UAS-bor*^{WT}, or *UAS-bor*^{R534W}. Scale bars represent 500 nm.

(C) Quantification of ATP5A signal intensity in muscle of larvae carrying *C57-Gal4*, together with *UAS-empty*, *UAS-bor*^{WT}, or *UAS-bor*^{R534W} from confocal images (A).

(D) Quantification of mitochondrial length in muscle of larvae carrying *C57-Gal4*, together with *UAS-empty*, *UAS-bor*^{WT}, or *UAS-bor*^{R534W} from TEM images (B).

(E) TEM of fibroblasts from an affected individual (BAB8644, *ATAD3A*$^{p.R528W/+}$) and control (*ATAD3A*$^{+/+}$) fibroblasts. Scale bars represent 500 nm.

(F) Quantification of mitophagic vesicles (E, arrows) among all vesicles in affected (BAB8644, *ATAD3A*$^{R528W/+}$) and control (*ATAD3A*$^{+/+}$) fibroblasts.

(G) TEM of muscle from first instar larvae for *bor* mutants (*bor*^{c05496}*/Df (3R)Excel7329*) and control (*bor*^{c05496}/+). Scale bars represent 500 nm.

(H) Quantification of mitochondria per area in *bor* mutants (*bor*^{c05496}*/Df (3R)Excel7329*) and control (*bor*^{c05496}/+).

(C, D, F, H) Error bars indicate SEM. p values were calculated by Student's t test. *$p < 0.05$. ***$p < 0.001$. N.S. indicates not statistically significant.

The features associated with the biallelic SNV identified in two siblings include ataxia, epilepsy, and congenital cataracts, while the compound heterozygous CNVs conferred a more severe phenotype of respiratory insufficiency at birth, cloudy corneas, hypoplastic cerebellum and brainstem, and seizures. Monoallelic and biallelic pathogenic variation at a single locus has been observed for numerous genes, including mitochondrial genes (e.g., *OPA1* [MIM: 605290], *SLC25A4* [MIM: 103220], *AARS* [MIM: 601065], *EMC1* [MIM: 616846], *MAB21L2* [MIM: 604357], and *NALCN* [MIM: 611549]).[9,58–63] There is often a difference in severity of phenotype between the monoallelic and biallelic forms of disease, although in many cases, the same organ systems are involved. In the case of *ATAD3A*, there is primarily involvement of the nervous system and the eye in both monoallelic and biallelic forms.

The ExAC constraint metric for loss of function is 0.04, indicating a high tolerance for heterozygous loss-of-function alleles. Indeed, individuals harboring a heterozygous deletion involving the *ATAD3* genes (i.e., parents in family 7) are unaffected. These data suggest a dominant-negative pathogenic mechanism or a gain-of-function mechanism for the recurrent de novo variant rather than haploinsufficiency. The data from *Drosophila* show that overexpression of a wild-type cDNA, one form of a gain-of-function experiment, does not affect viability and leads to an expansion of mitochondrial size. However, expression of the de novo variant in many tissues in flies is toxic and leads to death. The observed phenotype in these tissues phenocopies the null mutant and yields effects opposite to those seen with overexpression of the wild-type cDNA. Hence, experimental evidence indicates that ATAD3A p.Arg528Trp behaves as a dominant-negative, or antimorphic, allele. This conclusion is supported further by the proposed oligomeric formation of ATAD3 proteins.[15]

Although most species have only one *ATAD3* gene locus, primates have three *ATAD3* paralogs (*ATAD3A*, *ATAD3B*, *ATAD3C*), which appear to have evolved by duplication of a single precursor gene. In humans, the three genes are located in tandem on chromosome 1p36.33 (Figure 1E). Multiple isoforms of the three *ATAD3* genes are generated by transcriptional and post-transcriptional events. The major *ATAD3A* isoform, p66, is ubiquitously expressed, whereas the major *ATAD3B* isoform, p67, was specifically detected in embryo muscle, placenta, and adult brain and heart. *ATAD3C* is missing four exons as compared to *ATAD3A*, suggesting that it may be a pseudogene. In the mouse, a single *Atad3* gene is located on murine chromosome 4 and encodes a major ubiquitous isoform and several smaller tissue- and/or temporal-specific isoforms.[23] ATAD3 function is essential in the mouse for early post-implantation development. ATAD3-deficient embryos die around E7.5 due to growth retardation and a defective development of the trophoblast lineage; heterozygotes seem unaffected.[22] Given the severe phenotype and respiratory insufficiency of family 7, II-1, it may be surmised that biallelic deletions involving *ATAD3A* will lead to fetal demise. The potential salvage of lethality in this individual during development by a theoretical fusion protein extending from ATAD3B to ATAD3A and under control of the *ATAD3B* promoter, active during embryonic development,[23,64] warrants further investigation. Moreover, the potential embryonic lethality of the homozygous ~68 kb *ATAD3C-ATAD3A* allele could distort Mendelian expectations despite the observed relatively high (~1.5%) carrier frequency in the white population.

ATAD3A has two coiled-coil domains with high oligomerization probability within the N terminus, followed by a predicted transmembrane segment in the central part of the molecule and a conserved ATPase domain in the C terminus (Figure 1E).[15,23] Oligomerization of ATAD3A monomers is further supported by findings showing that other AAA proteins assemble as hexameric rings.[65] Studies in human U373 cells demonstrated that defective ATP-binding ATAD3A mutants interfere with normal oligomer functions and lead to fragmentation of mitochondria.[15] In the current study, we observed a dramatic loss of mitochondria in motor neurons of transgenic mutant flies (Figures 5B–5E), highly aberrant mitochondrial morphology, and an increase in autophagic intermediates in the fly muscle (Figure S12). Moreover, overexpression of wild-type *bor* resulted in an increased number of large elongated mitochondria (Figures 6B and 6D) whereas TEM of homozygous null flies showed a dramatic decrease in size and number of mitochondria (Figures 6G and 6H). Finally, fibroblasts from an affected individual harboring the p.Arg528Trp variant showed a significant increase in mitophagy (Figures 6E, 6F, and S13) and a reduction, though not statistically significant, in mitochondrial content (Figure S14). The aggregate data suggest that the production of small aberrant mitochondria probably results in increased mitophagy and a significant reduction of mitochondrial content. The molecular mechanisms remain to be elucidated.

In summary, we have identified monoallelic and biallelic variation involving both SNVs and CNVs at the *ATAD3A* locus. We propose that the dominant p.Arg528Trp variant disturbs ATAD3A function by a dominant-negative mechanism, while the recessive CNVs lead to infantile lethality through loss of ATAD3A function. These data suggest an allelic series with decreasing severity: c.1582C>T (p.Arg528Trp) (antimorph) > *ATAD3A* deletion CNV (null) > c.158C>T (p.Thr53Ile) (hypomorph). The previously described function of ATAD3A in mitochondrial dynamics and its co-immunoprecipitation with MFN2 and OPA1, in conjunction with the phenotypic and functional data presented herein, indicates that ATAD3A is essential in humans.

Accession Numbers

The ClinVar accession numbers for the DNA variant data reported in this paper are SCV000267601, SCV000267602, SCV000267603, and SCV000267604.

Supplemental Data

Supplemental Data include detailed clinical case reports, 15 figures, and 4 tables and can be found with this article online at http://dx.doi.org/10.1016/j.ajhg.2016.08.007.

Conflicts of Interest

J.R.L. has stock ownership in 23andMe, is a paid consultant for Regeneron Pharmaceuticals, has stock options in Lasergen, Inc., is a member of the Scientific Advisory Board of Baylor Genetics, and is a co-inventor on multiple United States and European patents related to molecular diagnostics for inherited neuropathies, eye diseases, and bacterial genomic fingerprinting. The Department of Molecular and Human Genetics at Baylor College of Medicine derives revenue from the chromosomal microarray analysis (CMA) and clinical exome sequencing offered at Baylor Genetics.

Acknowledgments

We thank the families for their collaboration and participation in this study. This work was supported in part by the US National Human Genome Research Institute/National Heart Lung and Blood Institute Baylor Hopkins Center for Mendelian Genomics (NHGRI/NHLBI, U54HG006542), the Intellectual Developmental Disabilities Research Center, IDDRC (NICHD HD083092, Clinical Translational Core), and the NHGRI/NHLBI University of Washington Center for Mendelian Genomics (2UM1HG006493). This work was also supported in part by the National Institute of Neurological Disease and Stroke (NINDS, RO1NS058529) to J.R.L. T.H. and J.E.P. are supported by the NIH/NIGMS T32 GM07526 Medical Genetics Research Fellowship Program. C. Garone is supported by European Commission Project 705560, Marie Curie Individual Fellowship. H.J.B. is supported by the Undiagnosed Diseases Network (UDN, 1U54NS093793-01). R.A.L. is supported in part by the Genetic Resource Association of Texas (GReAT), Houston, Texas. D.M. Martin is supported by the NIH (R01 DC009410) and the Dointa B. Sullivan, MD Research Professorship.

Received: June 6, 2016
Accepted: August 4, 2016
Published: September 15, 2016

Web Resources

1000 Genomes, http://www.1000genomes.org
Atherosclerosis Risk in Communities Study (ARIC), http://drupal.cscc.unc.edu/aric/
Baylor Genetics, http://www.bmgl.com
CADD, http://cadd.gs.washington.edu/
ConSurf, consurf.tau.ac.il
Database of Genomic Variants (DGV), http://dgv.tcag.ca/dgv/app/home
Ensembl Genome Browser, http://www.ensembl.org/index.html
ExAC Browser, http://exac.broadinstitute.org/
GeneMatcher, https://genematcher.org/
HMZDelFinder, https://github.com/BCM-Lupskilab/HMZDelFinder
NHLBI Exome Sequencing Project (ESP) Exome Variant Server, http://evs.gs.washington.edu/EVS/
OMIM, http://www.omim.org/
PyMOL, http://www.pymol.org
R statistical software, http://www.r-project.org/
SIFT, http://sift.bii.a-star.edu.sg/

References

1. Mishra, P., and Chan, D.C. (2014). Mitochondrial dynamics and inheritance during cell division, development and disease. Nat. Rev. Mol. Cell Biol. *15*, 634–646.
2. Niemann, A., Ruegg, M., La Padula, V., Schenone, A., and Suter, U. (2005). Ganglioside-induced differentiation associated protein 1 is a regulator of the mitochondrial network: new implications for Charcot-Marie-Tooth disease. J. Cell Biol. *170*, 1067–1078.
3. Pareyson, D., Saveri, P., Sagnelli, A., and Piscosquito, G. (2015). Mitochondrial dynamics and inherited peripheral nerve diseases. Neurosci. Lett. *596*, 66–77.
4. Züchner, S., Mersiyanova, I.V., Muglia, M., Bissar-Tadmouri, N., Rochelle, J., Dadali, E.L., Zappia, M., Nelis, E., Patitucci, A., Senderek, J., et al. (2004). Mutations in the mitochondrial GTPase mitofusin 2 cause Charcot-Marie-Tooth neuropathy type 2A. Nat. Genet. *36*, 449–451.
5. Züchner, S., De Jonghe, P., Jordanova, A., Claeys, K.G., Guergueltcheva, V., Cherninkova, S., Hamilton, S.R., Van Stavern, G., Krajewski, K.M., Stajich, J., et al. (2006). Axonal neuropathy with optic atrophy is caused by mutations in mitofusin 2. Ann. Neurol. *59*, 276–281.
6. Verhoeven, K., Claeys, K.G., Züchner, S., Schröder, J.M., Weis, J., Ceuterick, C., Jordanova, A., Nelis, E., De Vriendt, E., Van Hul, M., et al. (2006). *MFN2* mutation distribution and genotype/phenotype correlation in Charcot-Marie-Tooth type 2. Brain *129*, 2093–2102.
7. Rouzier, C., Bannwarth, S., Chaussenot, A., Chevrollier, A., Verschueren, A., Bonello-Palot, N., Fragaki, K., Cano, A., Pouget, J., Pellissier, J.F., et al. (2012). The *MFN2* gene is responsible for mitochondrial DNA instability and optic atrophy 'plus' phenotype. Brain *135*, 23–34.
8. Yu-Wai-Man, P., Griffiths, P.G., Gorman, G.S., Lourenco, C.M., Wright, A.F., Auer-Grumbach, M., Toscano, A., Musumeci, O., Valentino, M.L., Caporali, L., et al. (2010). Multi-system neurological disease is common in patients with *OPA1* mutations. Brain *133*, 771–786.
9. Spiegel, R., Saada, A., Flannery, P.J., Burté, F., Soiferman, D., Khayat, M., Eisner, V., Vladovski, E., Taylor, R.W., Bindoff, L.A., et al. (2016). Fatal infantile mitochondrial encephalomyopathy, hypertrophic cardiomyopathy and optic atrophy associated with a homozygous *OPA1* mutation. J. Med. Genet. *53*, 127–131.
10. Chao, Y.H., Robak, L.A., Xia, F., Koenig, M.K., Adesina, A., Bacino, C.A., Scaglia, F., Bellen, H.J., and Wangler, M.F. (2016). Missense variants in the middle domain of DNM1L in cases of infantile encephalopathy alter peroxisomes and mitochondria when assayed in *Drosophila*. Hum. Mol. Genet. *25*, 1846–1856.
11. Waterham, H.R., Koster, J., van Roermund, C.W., Mooyer, P.A., Wanders, R.J., and Leonard, J.V. (2007). A lethal defect of mitochondrial and peroxisomal fission. N. Engl. J. Med. *356*, 1736–1741.
12. Shahni, R., Cale, C.M., Anderson, G., Osellame, L.D., Hambleton, S., Jacques, T.S., Wedatilake, Y., Taanman, J.W., Chan, E., Qasim, W., et al. (2015). Signal transducer and activator of transcription 2 deficiency is a novel disorder of mitochondrial fission. Brain *138*, 2834–2846.

13. Abrams, A.J., Hufnagel, R.B., Rebelo, A., Zanna, C., Patel, N., Gonzalez, M.A., Campeanu, I.J., Griffin, L.B., Groenewald, S., Strickland, A.V., et al. (2015). Mutations in *SLC25A46*, encoding a UGO1-like protein, cause an optic atrophy spectrum disorder. Nat. Genet. *47*, 926–932.
14. Niemann, A., Wagner, K.M., Ruegg, M., and Suter, U. (2009). *GDAP1* mutations differ in their effects on mitochondrial dynamics and apoptosis depending on the mode of inheritance. Neurobiol. Dis. *36*, 509–520.
15. Gilquin, B., Taillebourg, E., Cherradi, N., Hubstenberger, A., Gay, O., Merle, N., Assard, N., Fauvarque, M.O., Tomohiro, S., Kuge, O., and Baudier, J. (2010). The AAA+ ATPase ATAD3A controls mitochondrial dynamics at the interface of the inner and outer membranes. Mol. Cell. Biol. *30*, 1984–1996.
16. He, J., Cooper, H.M., Reyes, A., Di Re, M., Sembongi, H., Litwin, T.R., Gao, J., Neuman, K.C., Fearnley, I.M., Spinazzola, A., et al. (2012). Mitochondrial nucleoid interacting proteins support mitochondrial protein synthesis. Nucleic Acids Res. *40*, 6109–6121.
17. Issop, L., Fan, J., Lee, S., Rone, M.B., Basu, K., Mui, J., and Papadopoulos, V. (2015). Mitochondria-associated membrane formation in hormone-stimulated Leydig cell steroidogenesis: role of ATAD3. Endocrinology *156*, 334–345.
18. Rone, M.B., Midzak, A.S., Issop, L., Rammouz, G., Jagannathan, S., Fan, J., Ye, X., Blonder, J., Veenstra, T., and Papadopoulos, V. (2012). Identification of a dynamic mitochondrial protein complex driving cholesterol import, trafficking, and metabolism to steroid hormones. Mol. Endocrinol. *26*, 1868–1882.
19. Teng, Y., Ren, X., Li, H., Shull, A., Kim, J., and Cowell, J.K. (2016). Mitochondrial ATAD3A combines with GRP78 to regulate the WASF3 metastasis-promoting protein. Oncogene *35*, 333–343.
20. You, W.C., Chiou, S.H., Huang, C.Y., Chiang, S.F., Yang, C.L., Sudhakar, J.N., Lin, T.Y., Chiang, I.P., Shen, C.C., Cheng, W.Y., et al. (2013). Mitochondrial protein ATPase family, AAA domain containing 3A correlates with radioresistance in glioblastoma. Neuro-oncol. *15*, 1342–1352.
21. Fang, H.Y., Chang, C.L., Hsu, S.H., Huang, C.Y., Chiang, S.F., Chiou, S.H., Huang, C.H., Hsiao, Y.T., Lin, T.Y., Chiang, I.P., et al. (2010). ATPase family AAA domain-containing 3A is a novel anti-apoptotic factor in lung adenocarcinoma cells. J. Cell Sci. *123*, 1171–1180.
22. Goller, T., Seibold, U.K., Kremmer, E., Voos, W., and Kolanus, W. (2013). Atad3 function is essential for early post-implantation development in the mouse. PLoS ONE *8*, e54799.
23. Li, S., Lamarche, F., Charton, R., Delphin, C., Gires, O., Hubstenberger, A., Schlattner, U., and Rousseau, D. (2014). Expression analysis of *ATAD3* isoforms in rodent and human cell lines and tissues. Gene *535*, 60–69.
24. Hoffmann, M., Bellance, N., Rossignol, R., Koopman, W.J., Willems, P.H., Mayatepek, E., Bossinger, O., and Distelmaier, F. (2009). *C. elegans ATAD-3* is essential for mitochondrial activity and development. PLoS ONE *4*, e7644.
25. Yang, Y., Muzny, D.M., Xia, F., Niu, Z., Person, R., Ding, Y., Ward, P., Braxton, A., Wang, M., Buhay, C., et al. (2014). Molecular findings among patients referred for clinical whole-exome sequencing. JAMA *312*, 1870–1879.
26. Reid, J.G., Carroll, A., Veeraraghavan, N., Dahdouli, M., Sundquist, A., English, A., Bainbridge, M., White, S., Salerno, W., Buhay, C., et al. (2014). Launching genomics into the cloud: deployment of Mercury, a next generation sequence analysis pipeline. BMC Bioinformatics *15*, 30.
27. Challis, D., Yu, J., Evani, U.S., Jackson, A.R., Paithankar, S., Coarfa, C., Milosavljevic, A., Gibbs, R.A., and Yu, F. (2012). An integrative variant analysis suite for whole exome next-generation sequencing data. BMC Bioinformatics *13*, 8.
28. Li, H., Handsaker, B., Wysoker, A., Fennell, T., Ruan, J., Homer, N., Marth, G., Abecasis, G., and Durbin, R.; 1000 Genome Project Data Processing Subgroup (2009). The Sequence Alignment/Map format and SAMtools. Bioinformatics *25*, 2078–2079.
29. Wang, K., Li, M., and Hakonarson, H. (2010). ANNOVAR: functional annotation of genetic variants from high-throughput sequencing data. Nucleic Acids Res. *38*, e164.
30. Sobreira, N., Schiettecatte, F., Valle, D., and Hamosh, A. (2015). GeneMatcher: a matching tool for connecting investigators with an interest in the same gene. Hum. Mutat. *36*, 928–930.
31. Yang, J., Yan, R., Roy, A., Xu, D., Poisson, J., and Zhang, Y. (2015). The I-TASSER Suite: protein structure and function prediction. Nat. Methods *12*, 7–8.
32. Zhang, Y. (2008). I-TASSER server for protein 3D structure prediction. BMC Bioinformatics *9*, 40.
33. Ashkenazy, H., Erez, E., Martz, E., Pupko, T., and Ben-Tal, N. (2010). ConSurf 2010: calculating evolutionary conservation in sequence and structure of proteins and nucleic acids. Nucleic Acids Res. *38*, W529-33.
34. Bugiani, M., Invernizzi, F., Alberio, S., Briem, E., Lamantea, E., Carrara, F., Moroni, I., Farina, L., Spada, M., Donati, M.A., et al. (2004). Clinical and molecular findings in children with complex I deficiency. Biochim. Biophys. Acta *1659*, 136–147.
35. Fromer, M., Moran, J.L., Chambert, K., Banks, E., Bergen, S.E., Ruderfer, D.M., Handsaker, R.E., McCarroll, S.A., O'Donovan, M.C., Owen, M.J., et al. (2012). Discovery and statistical genotyping of copy-number variation from whole-exome sequencing depth. Am. J. Hum. Genet. *91*, 597–607.
36. Parsons, J.D. (1995). Miropeats: graphical DNA sequence comparisons. Comput. Appl. Biosci. *11*, 615–619.
37. Parks, A.L., Cook, K.R., Belvin, M., Dompe, N.A., Fawcett, R., Huppert, K., Tan, L.R., Winter, C.G., Bogart, K.P., Deal, J.E., et al. (2004). Systematic generation of high-resolution deletion coverage of the *Drosophila melanogaster* genome. Nat. Genet. *36*, 288–292.
38. Bischof, J., Maeda, R.K., Hediger, M., Karch, F., and Basler, K. (2007). An optimized transgenesis system for *Drosophila* using germ-line-specific phiC31 integrases. Proc. Natl. Acad. Sci. USA *104*, 3312–3317.
39. Venken, K.J., He, Y., Hoskins, R.A., and Bellen, H.J. (2006). P [acman]: a BAC transgenic platform for targeted insertion of large DNA fragments in *D. melanogaster*. Science *314*, 1747–1751.
40. Bellen, H., and Budnik, V. (2000). The Neuromuscular Junction (New York: Cold Spring Harbor Laboratory Press).
41. Cooper, D.N., Mort, M., Stenson, P.D., Ball, E.V., and Chuzhanova, N.A. (2010). Methylation-mediated deamination of 5-methylcytosine appears to give rise to mutations causing human inherited disease in CpNpG trinucleotides, as well as in CpG dinucleotides. Hum. Genomics *4*, 406–410.
42. Cooper, D.N., and Krawczak, M. (1989). Cytosine methylation and the fate of CpG dinucleotides in vertebrate genomes. Hum. Genet. *83*, 181–188.
43. Coulondre, C., Miller, J.H., Farabaugh, P.J., and Gilbert, W. (1978). Molecular basis of base substitution hotspots in *Escherichia coli*. Nature *274*, 775–780.

44. Posey, J.E., Rosenfeld, J.A., James, R.A., Bainbridge, M., Niu, Z., Wang, X., Dhar, S., Wiszniewski, W., Akdemir, Z.H., Gambin, T., et al. (2016). Molecular diagnostic experience of whole-exome sequencing in adult patients. Genet. Med. *18*, 678–685.
45. Farwell, K.D., Shahmirzadi, L., El-Khechen, D., Powis, Z., Chao, E.C., Tippin Davis, B., Baxter, R.M., Zeng, W., Mroske, C., Parra, M.C., et al. (2015). Enhanced utility of family-centered diagnostic exome sequencing with inheritance model-based analysis: results from 500 unselected families with undiagnosed genetic conditions. Genet. Med. *17*, 578–586.
46. Yang, Y., Muzny, D.M., Reid, J.G., Bainbridge, M.N., Willis, A., Ward, P.A., Braxton, A., Beuten, J., Xia, F., Niu, Z., et al. (2013). Clinical whole-exome sequencing for the diagnosis of mendelian disorders. N. Engl. J. Med. *369*, 1502–1511.
47. Campbell, I.M., Shaw, C.A., Stankiewicz, P., and Lupski, J.R. (2015). Somatic mosaicism: implications for disease and transmission genetics. Trends Genet. *31*, 382–392.
48. Campbell, I.M., Stewart, J.R., James, R.A., Lupski, J.R., Stankiewicz, P., Olofsson, P., and Shaw, C.A. (2014). Parent of origin, mosaicism, and recurrence risk: probabilistic modeling explains the broken symmetry of transmission genetics. Am. J. Hum. Genet. *95*, 345–359.
49. Carvalho, C.M., and Lupski, J.R. (2016). Mechanisms underlying structural variant formation in genomic disorders. Nat. Rev. Genet. *17*, 224–238.
50. Dittwald, P., Gambin, T., Szafranski, P., Li, J., Amato, S., Divon, M.Y., Rodríguez Rojas, L.X., Elton, L.E., Scott, D.A., Schaaf, C.P., et al. (2013). NAHR-mediated copy-number variants in a clinical population: mechanistic insights into both genomic disorders and Mendelizing traits. Genome Res. *23*, 1395–1409.
51. Cooper, G.M., Coe, B.P., Girirajan, S., Rosenfeld, J.A., Vu, T.H., Baker, C., Williams, C., Stalker, H., Hamid, R., Hannig, V., et al. (2011). A copy number variation morbidity map of developmental delay. Nat. Genet. *43*, 838–846.
52. Uddin, M., Thiruvahindrapuram, B., Walker, S., Wang, Z., Hu, P., Lamoureux, S., Wei, J., MacDonald, J.R., Pellecchia, G., Lu, C., et al. (2015). A high-resolution copy-number variation resource for clinical and population genetics. Genet. Med. *17*, 747–752.
53. Greenberg, F., Lewis, R.A., Potocki, L., Glaze, D., Parke, J., Killian, J., Murphy, M.A., Williamson, D., Brown, F., Dutton, R., et al. (1996). Multi-disciplinary clinical study of Smith-Magenis syndrome (deletion 17p11.2). Am. J. Med. Genet. *62*, 247–254.
54. Li, S., Yao, Y., Xu, R., Pesenti, S., Cottet-Rousselle, C., Rieusset, J., Tokarska-Schlattner, M., Liao, K., Schlattner, U., and Rousseau, D. (2014). ATAD3 is a limiting factor in mitochondrial biogenesis and adipogenesis of white adipocyte-like 3T3-L1 cells. Mol. Cell. Biol. Published online April 14, 2014. http://dx.doi.org/10.1128/MCB.01170-13.
55. Buzin, C.H., Feng, J., Yan, J., Scaringe, W., Liu, Q., den Dunnen, J., Mendell, J.R., and Sommer, S.S. (2005). Mutation rates in the dystrophin gene: a hotspot of mutation at a CpG dinucleotide. Hum. Mutat. *25*, 177–188.
56. Muona, M., Berkovic, S.F., Dibbens, L.M., Oliver, K.L., Maljevic, S., Bayly, M.A., Joensuu, T., Canafoglia, L., Franceschetti, S., Michelucci, R., et al. (2015). A recurrent de novo mutation in *KCNC1* causes progressive myoclonus epilepsy. Nat. Genet. *47*, 39–46.
57. Schuurs-Hoeijmakers, J.H., Oh, E.C., Vissers, L.E., Swinkels, M.E., Gilissen, C., Willemsen, M.A., Holvoet, M., Steehouwer, M., Veltman, J.A., de Vries, B.B., et al. (2012). Recurrent de novo mutations in *PACS1* cause defective cranial-neural-crest migration and define a recognizable intellectual-disability syndrome. Am. J. Hum. Genet. *91*, 1122–1127.
58. Kaukonen, J.A., Amati, P., Suomalainen, A., Rötig, A., Piscaglia, M.-G., Salvi, F., Weissenbach, J., Fratta, G., Comi, G., Peltonen, L., and Zeviani, M. (1996). An autosomal locus predisposing to multiple deletions of mtDNA on chromosome 3p. Am. J. Hum. Genet. *58*, 763–769.
59. Palmieri, L., Alberio, S., Pisano, I., Lodi, T., Meznaric-Petrusa, M., Zidar, J., Santoro, A., Scarcia, P., Fontanesi, F., Lamantea, E., et al. (2005). Complete loss-of-function of the heart/muscle-specific adenine nucleotide translocator is associated with mitochondrial myopathy and cardiomyopathy. Hum. Mol. Genet. *14*, 3079–3088.
60. Simons, C., Griffin, L.B., Helman, G., Golas, G., Pizzino, A., Bloom, M., Murphy, J.L., Crawford, J., Evans, S.H., Topper, S., et al. (2015). Loss-of-function alanyl-tRNA synthetase mutations cause an autosomal-recessive early-onset epileptic encephalopathy with persistent myelination defect. Am. J. Hum. Genet. *96*, 675–681.
61. Harel, T., Yesil, G., Bayram, Y., Coban-Akdemir, Z., Charng, W.L., Karaca, E., Al Asmari, A., Eldomery, M.K., Hunter, J.V., Jhangiani, S.N., et al.; Baylor-Hopkins Center for Mendelian Genomics (2016). Monoallelic and biallelic variants in *EMC1* identified in individuals with global developmental delay, hypotonia, scoliosis and cerebellar atrophy. Am. J. Hum. Genet. *98*, 562–570.
62. Rainger, J., Pehlivan, D., Johansson, S., Bengani, H., Sanchez-Pulido, L., Williamson, K.A., Ture, M., Barker, H., Rosendahl, K., Spranger, J., et al.; UK10K; Baylor-Hopkins Center for Mendelian Genomics (2014). Monoallelic and biallelic mutations in *MAB21L2* cause a spectrum of major eye malformations. Am. J. Hum. Genet. *94*, 915–923.
63. Chong, J.X., McMillin, M.J., Shively, K.M., Beck, A.E., Marvin, C.T., Armenteros, J.R., Buckingham, K.J., Nkinsi, N.T., Boyle, E.A., Berry, M.N., et al.; University of Washington Center for Mendelian Genomics (2015). De novo mutations in *NALCN* cause a syndrome characterized by congenital contractures of the limbs and face, hypotonia, and developmental delay. Am. J. Hum. Genet. *96*, 462–473.
64. Merle, N., Féraud, O., Gilquin, B., Hubstenberger, A., Kieffer-Jacquinot, S., Assard, N., Bennaceur-Griscelli, A., Honnorat, J., and Baudier, J. (2012). ATAD3B is a human embryonic stem cell specific mitochondrial protein, re-expressed in cancer cells, that functions as dominant negative for the ubiquitous ATAD3A. Mitochondrion *12*, 441–448.
65. Langer, T., Käser, M., Klanner, C., and Leonhard, K. (2001). AAA proteases of mitochondria: quality control of membrane proteins and regulatory functions during mitochondrial biogenesis. Biochem. Soc. Trans. *29*, 431–436.

The American Journal of Human Genetics, Volume *99*

Supplemental Data

Recurrent De Novo and Biallelic Variation of *ATAD3A*, Encoding a Mitochondrial Membrane Protein, Results in Distinct Neurological Syndromes

Tamar Harel, Wan Hee Yoon, Caterina Garone, Shen Gu, Zeynep Coban-Akdemir, Mohammad K. Eldomery, Jennifer E. Posey, Shalini N. Jhangiani, Jill A. Rosenfeld, Megan T. Cho, Stephanie Fox, Marjorie Withers, Stephanie M. Brooks, Theodore Chiang, Lita Duraine, Serkan Erdin, Bo Yuan, Yunru Shao, Elie Moussallem, Costanza Lamperti, Maria A. Donati, Joshua D. Smith, Heather M. McLaughlin, Christine M. Eng, Magdalena Walkiewicz, Fan Xia, Tommaso Pippucci, Pamela Magini, Marco Seri, Massimo Zeviani, Michio Hirano, Jill V. Hunter, Myriam Srour, Stefano Zanigni, Richard Alan Lewis, Donna M. Muzny, Timothy E. Lotze, Eric Boerwinkle, Baylor-Hopkins Center for Mendelian Genomics, University of Washington Center for Mendelian Genomics, Richard A. Gibbs, Scott E. Hickey, Brett H. Graham, Yaping Yang, Daniela Buhas, Donna M. Martin, Lorraine Potocki, Claudio Graziano, Hugo J. Bellen, and James R. Lupski

CLINICAL DESCRIPTIONS

Family 1, II-2

We report a 9-year-old female (BH5923_1, designated Family 1, II-2 in **Figure 1A**) who presented with delayed motor development and hypotonia. She was born to a 28 -year old gravida 2, para 1->2 mother and a 30 -year old father at 42 weeks gestation after an overall uncomplicated pregnancy, via vaginal delivery at a birthweight of 3005 grams (~10th percentile). Motor development was delayed, with crawling at 12 months and walking with a walker at 2 years. Language development was also delayed, with her first words between 18 and 24 months and sentences at about 30 months. She had difficulty feeding since early infancy; a swallow function study revealed oropharyngeal dysphagia and poor clearing of the oropharynx. Medical history was further significant for mild sleep apnea, a history of sleep disturbance, recurrent otitis media, recurrent urinary tract infections, nosebleeds at an early age and hip dysplasia s/p surgery. At 9 years of age, her head circumference was 51.4 cm (40th percentile), height 116.4 cm (Z score = -3.1), and weight 19.6 kg (Z score = -2.94). She was nondysmorphic. Physical examination revealed general hypotonia, muscle wasting most pronounced in the distal extremities with a 'stork leg' deformity of both calves, and poor development of the hypothenar and thenar eminences. She exhibited an abnormal, spastic crouched gait when walking with crutches. Patellar deep tendon reflexes (DTRs) were brisk, but ankle reflexes could not be elicited. DTRs of the upper extremities were normal. No clonus was elicited. Brain magnetic resonance imaging (MRI) showed a Chiari malformation, and MR spectroscopy and spine MRI were normal. Ophthalmology exam revealed temporal optic atrophy and

myopia. EMG and NCV studies were consistent with axonal neuropathy (**Table S1**). Muscle biopsy was not obtained. Previous laboratory studies included chromosome analysis, plasma acylcarnitine profile, plasma amino acids, urine organic acids, lactate, creatine kinase (CK), and thyroid function studies all of which were reported normal. Array comparative genome hybridization (CGH) detected a paternally inherited 0.288 Mb gain on Xq24 including *UPF3B*; mutations in the latter have been associated with X-linked syndromic intellectual disability in males, and this finding is of unclear significance in females. Targeted testing for *MPZ* and *EGR2* was negative. Thus, the overall clinical diagnosis was of possible upper motor neuron involvement and axonal neuropathy with a negative work-up. Whole exome sequencing of the proband and both parents revealed a heterozygous variant in *ATAD3A* (g. chr1:1464679 C>T [hg19]; GenBank:NM_001170535.1; c.1582C>T; p.Arg528Trp) which was not present in either parent. Sanger sequencing confirmed that the variant likely arose *de novo* in the affected individual (**Figure 1B**). The variant arose in a CpG dinucleotide within a CpG island of 298 bp, with a 15.4% percent CpG (ratio of observed to expected CpG: 0.67) (UCSC Genome Browser CpG track; Santa Cruz, CA). The variant was not seen in any publically available database nor in our internal database.

Family 2, II-4

The second individual (designated Family 2, II-4 in **Figure 1A**) was a 5-year-old female with developmental delay, truncal hypotonia and peripheral spasticity. Motor development was delayed, with no independent walking at 5 years of age. Speech was delayed, and she had borderline normal hearing. Cognitive development

was moderately delayed. She had difficulty feeding and required G-tube feeding. In addition, she had sleep apnea, slight acetabular dysplasia and a dislocated hip. At 5 years of age, her head circumference was at the 59th percentile, height Z score was -2.5, and weight was 25th percentile. She was otherwise nondysmorphic. Physical exam revealed truncal hypotonia, peripheral spasticity, and bilateral talipes equinovalgus (**Figure 2**). Nystagmus, esotropia, myopia, and astigmatism were evident on ophthalmologic exam. Brain MRI, echocardiogram and renal ultrasound were normal. EMG and NCV studies were consistent with axonal neuropathy (**Table S1**). Lactate and pyruvate were mildly elevated; creatine kinase (CK) was normal. Muscle biopsy showed no diagnostic abnormalities, and she had normal sequencing and deletion analysis of the mitochondrial genome. Mitochondrial respiratory chain enzyme analysis in muscle showed a deficiency of complex I plus III activity. Chromosome analysis and array CGH were normal.

Whole exome sequencing was undertaken on the proband and her parents. Genomic DNA was extracted from whole blood, and exome sequencing at GeneDx was performed on exon targets isolated by capture with the Agilent SureSelect Human All Exon V4 (50 Mb) kit or the Clinical Research Exome kit (Agilent Technologies, Santa Clara, CA). Sequencing technology and variant interpretation protocol were done as previously described.[1] The general assertion criteria for variant classification are publicly available on the GeneDx ClinVar submission page (http://www.ncbi.nlm.nih.gov/clinvar/submitters/26957/). A heterozygous variant was identified in *ATAD3A* (g. chr1:1464679 C>T [hg19]; GenBank:NM_001170535.1; c.1582C>T; p.Arg528Trp) which was not present in either parent, and Sanger sequencing confirmed that this variant likely arose *de novo* in the affected individual.

Family 3, II-1

The third individual (Family 3, II-1 in **Figure 1A**) was a 3-year-old male with global developmental delay, borderline microcephaly (~3rd %ile), hypotonia with peripheral spasticity, feeding difficulties that resolved, and sleep abnormalities. He was non-ambulatory at age 3-years. Dysmorphic features included absent eyebrows, deep set eyes with esotropia, a triangular face, small mandibular region, beaked nose, and a high arched palate. Skeletal abnormalities included pectus carinatum and severe scoliosis. Neurological exam showed axial hypotonia with peripheral spasticity, and ophthalmology exam showed esotropia, optic nerve pallor, and macular hypoplasia. An echocardiogram revealed hypertrophic cardiomyopathy, initially detected at age 3 months. NCV studies showed peripheral neuropathy. Additionally, he had growth hormone deficiency, hypoplasia of optic nerves on MRI and possible cone-rod dysplasia. Lactate was intermittently elevated, and a mitochondrial condition was suspected.

Whole exome sequencing of the proband and both parents at GeneDx (see above) revealed a heterozygous variant in *ATAD3A* (g. chr1:1464679 C>T [hg19]; GenBank:NM_001170535.1; c.1582C>T; p.Arg528Trp) which was not present in either parent, and Sanger sequencing confirmed that this variant likely arose *de novo* in the affected individual.

Family 4, II-1

This individual (Family 4, II-1 in **Figure 1A**) was born to non-consanguineous Italian parents at term, after normal pregnancy and delivery (weight 2580 grams). Family history was positive for polyarthritis and congenital bicuspid aortic valve in the mother. No other disorders were reported. The proband presented with growth failure and emesis at 12 days of age. ECG and echocardiography revealed severe hypertrophic cardiomyopathy. At 4 months of age, she was admitted to the hospital for evaluation of severe developmental delay and failure to thrive. Height (54 cm), weight (3960 g) and head circumference (38.5 cm) were all below the 3rd centile. Facial features included low set ears, a triangular facies and micrognathia. Upon neurological evaluation she presented with truncal hypotonia and increased muscular tone in the extremities associated with dystonic movements and buccal dyskinesia. Neither eye contact nor head control were present. Metabolic workup revealed an increase in plasma alanine (394 micromol/l; normal 239-345) and lactic acid (39 mg/dl; normal 5-22), reduction of plasma citrulline (11.2 micromol/l; normal 17-53), and slight excretion of methylglutaconic acid (11UM/37UM; normal <9) and lactic acid (60UM, normal <25). Brain MRI showed enlargement of periencephalic spaces. Muscle biopsy showed lipid droplets, increased sarcolemmal COX activity, and reduction of succinate dehydrogenase (SDH) activity. Respiratory chain activities in muscle homogenate showed reduction of succinate dehydrogenase (SDH, II), citrate synthase (CS) and succinate cytochrome C reductase (II+III) (data not shown). Normal respiratory chain activities were found in skin derived fibroblasts of Family 4, II-1 (**Table S4)**. aCGH did not identify genomic imbalances. Treatments with β-blockers for cardiomyopathy and anti-oxidant/vitamin supplementation for mitochondrial abnormalities (thiamine, idebedenone, L-carnitine) were initiated. Feeding difficulties required nasogastric tube followed by gastrostomy placement.

During the clinical course, she experienced episodes of painful muscular rigidity (hypertonus) associated with vegetative symptoms. Neurophysiological studies (EEG) excluded epileptic seizures. In addition, she developed esotropia, optic nerve pallor, myopia, and oculo-motor incoordination confirmed by ophthalmologic evaluation at 18 months of age. At the last evaluation (5 years of age), height (85.5 cm, Z score -5.2), weight (10 kg, Z score -6.2), and head circumference (45.8 cm, Z score -3.3) were maintained below the 3rd centile. Few progresses in motor development were noticed: eye contact and social interaction, partial head control and intentional movement of the upper limbs. She could not yet sit unaided. Severe axial hypotonia and spasticity persisted.

Whole exome sequencing of the proband and both parents was performed at Columbia University Medical Center, Genome Facility. Samples were prepared using the Agilent SureSelectXT kit, captured with the Agilent All Exon v5 + UTRs library and sequenced on the Illumina HiSeq2500 instrument using a 2x100bp paired end run. NextGENe software was used to map reads to the whole genome sequence (version hg19) and generate variant call files (vcf files) with minimum coverage 10, minimum mutant rate 10% and homozygosis in >3 alleles. Variants in the coding and plus/minus 5p regions were filtered. Common SNVs with minor allele frequencies of >1% were filtered with the 1000 genome database and exome variant server, and when present in more than 20 cases from an in-house database (~1000 cases). A heterozygous variant in *ATAD3A* (g. chr1:1464679 C>T [hg19]; GenBank:NM_001170535.1; c.1582C>T; p.Arg528Trp) was identified in proband DNA and confirmed by Sanger sequencing, while excluded from parental samples. Interestingly, Sanger sequencing of the mother (Famisly 4, I-2) suggested possible low-level mosaicism in the maternal sample (**Figure S4**). The mother was unaffected

aside from cardiac arrhythmia diagnosed in childhood, for which she had pacemaker placement. Nerve conduction velocities in the mother were within normal limits.

Family 5, II-1

The fifth individual (Family 5, II-1 in **Figure 1A**) was a 23-month-old male born to a 27-year-old G3P3 female and a 44-year-old father. Pregnancy was complicated by oligohydramnios and decreased fetal movement, and vaginal delivery was induced at 37 weeks. Birthweight was 2800 grams, and there were no immediate complications. The individual was hypotonic since birth and had global developmental delay. At 23 months, he could roll, commando crawl and sit if placed in sitting position. He could not pull to stand nor cruise. He had language and speech delay, saying only two words at 23 months. Anthropometric measurements were as follows: height 82.9 cm (Z score=-1.38), weight 10.09 kg (Z score=-1.51), head circumference 48.1 cm (~50th %ile). Dysmorphic features included a high forehead, frontal bossing, deep set eyes, upslanting palpebral fissures, and micrognathia. Neurological exam was significant for axial hypotonia, head lag that improved over time, normal patellar DTRs (2+), and reduced ankle DTRs. Ophthalmology exam revealed high myopia (right sphere -7.50; left sphere -6.00) with normal optic nerves. Brain MRI showed mildly prominent extra-axial spaces and a persistent fetal left trigeminal artery. EMC/NCV studies were interpreted as essentially normal with the exception of somewhat small amplitudes for the lower extremity motor responses. Creatine kinase (CK) and echocardiography were normal. Array CGH followed by karyotyping revealed 47,XXY in all observed cells, indicative of Klinefelter syndrome. The hypotonia and developmental delay, which seemed far beyond what

would be expected with Klinefelter, prompted further genetic evaluation with trio whole exome sequencing. Whole exome sequencing of the proband and both parents revealed a heterozygous variant in *ATAD3A* (g. chr1:1464679 C>T [hg19]; GenBank:NM_001170535.1; c.1582C>T; p.Arg528Trp) which was not present in either parent, and Sanger sequencing confirmed that this variant likely arose *de novo* in the affected individual. An additional intronic variant in *ATAD3A* (chr1:1459214 G>A [hg19]; GenBank:NM_001170535.1; c.964-5G>A) was inherited from the father. RNA was not available to study effects on splicing, nor could the phase of the *de novo* variant with respect to the intronic variant be determined.

Family 6, II-1 and II-2

Family 6 included two affected siblings, a 26-year-old female (Family 6, II-1) and her 24-year-old brother (Family 6, II-2 in **Figure 1A**) of Italian descent. There was no known consanguinity, and family history was reportedly negative for ID, congenital cataracts, epilepsy or other early onset neurological conditions. The girl was born at term after an uneventful pregnancy. Measurements at birth were 3150g and 49cm, head circumference was 35cm. She showed developmental delay, with crawling at 10 months and unsupported walking at 22 months. She pronounced her first words at 24 months. Congenital nuclear cataract was diagnosed at three years (surgery performed at 6 years for the right eye, and at 7 years for the left eye). At four years, she started to show an ataxic gait and a neurological examination confirmed a mild limb ataxia with normal muscular tone and normal reflexes. At 6 years, she developed an absence seizure disorder with atonic crises managed with valproic acid. She had a mild delay in pubertal development, with menarche at 16 years. At a

subsequent neurological examination at 19 years, she showed hypotonia, reduced strength (more pronounced in lower limbs), intentional tremors of the upper limbs, and an ataxic gait. By 26 years, she had developed pes cavus deformity in her feet. An EKG and EEG at age 12 months were normal. EMG at age 5 years was normal, and bone age was delayed (3 years at chronological age 5 years). Echocardiogram at age 6 years was normal. Brain imaging performed at the age of 7 and 14 years showed a mildly progressive cerebellar atrophy. It was repeated again in her 20's (see below). IQ tests were performed at 9 years: WISC 61, Leiter 77.

The proband's affected brother was born at term after an uneventful pregnancy. Measurements at birth were 3500g and 50cm, head circumference was 35cm. He showed developmental delay, with crawling at 11 months and unsupported walking at 18 months. He pronounced his first words at 30 months. Zonular congenital cataract was diagnosed at three years (surgery performed at 4 for the right eye, at 5 for the left). At 7 years, he developed an absence seizure disorder managed initially with valproic acid and later with a combination of valproic acid and oxcarbazepine; the neurological examination revealed a normal muscular tone, normal reflexes and no ataxia, but the boy showed locomotor incoordination. At 10 years he underwent surgery for cryptorchidism. Stature at 12 years was 127.0cm (-3DS) and a mild GH deficiency was diagnosed. Somatotropin therapy was carried on from age 15 to age 19, with a final height of 169cm (target height 171cm). Puberty was delayed with onset of pubarche at age 16 years. Thyroid function, cortisol, prolactin and gonadotropins were normal. At a new neurological examination at 17 years, he showed hypotonia, reduced strength in upper and lower limbs, and an ataxic gait. EMG at age 3 years was normal, and an EKG at age 6 years resulted normal. Bone age was delayed (3.5 years at chronological age of 6 years). Brain MRI was

performed at the age of 6 years (normal) and at 13 and 24 years, when a mild cerebellar atrophy was reported. IQ tests were performed at 7 years: 102, although a language delay was present. Muscle histology and histochemistry showed lipid droplets.

At the age of 26 and 24 years respectively, individuals II-1 and II-2 from Family 6 underwent a standardized brain MR protocol on a 1.5 T scanner including axial FLAIR T2-weighted images, FSE coronal T_2-weighted images, volumetric T1-weighted fast spoiled gradient-echo (FSPGR) images (1 mm isotropic voxels), and axial DTI images of contiguous 3 mm slices using a single-shot SE-EPI sequence (25 diffusion gradient directions; b-value=900 s/mm2). Suppressed-water proton MR spectra (^{1}H-MRS) were acquired using the PRESS single-voxel localization sequence (PROBE).[2] Two Volumes of Interest (VOIs) were selected: left cerebellar hemisphere (6.0 mL; TR= 4000 ms, TE = 35 ms, and averaging 64 FIDs) and lateral ventricles for lactate evaluation [8.8 mL in Individual II-1 and 6.7 mL in Individual II-2 (Family 6); TR= 1500 ms, TE = 288 ms, and averaging 384 FIDs for each acquisition]. Metabolite's content was calculated using the fitting program LCModel v. 6.3[3,4] and expressed relatively to creatine.

On conventional brain MR, Individual II-1 (Family 6) presented a slight enlargement of the lateral and of the cerebral subarachnoid spaces, hypoplastic optic nerves and chiasma, a moderate enlargement of the fourth ventricle and of cerebellar hemispheres and vermis subarachnoid spaces (**Figure 2**), and a reduction of sagittal middle cerebellar peduncle diameter and coronal superior cerebellar peduncle diameter [7.0 mm and 2.1 mm, respectively; normal values (n.v.) > 8.10 mm and > 3.1 mm, respectively]. In addition, a pathological increase in mean diffusivity (MD) was detected in the dentate nucleus (0.90 x 10-3mm2/s; n.v. < 0.79 x 10-3mm2/s),

pons (0.95 x 10-3mm2/s; n.v. < 0.93 x 10-3mm2/s), superior cerebellar peduncles (1.05 x 10-3mm2/s; n.v. < 0.90 x 10-3mm2/s), vermis (1.44 x 10-3mm2/s; n.v. < 1.18 x 10-3mm2/s) and cerebellar hemispheres (1.22 x 10-3mm2/s; n.v. < 0.85 x 10-3mm2/s), indicating microstructural changes secondary to neurodegeneration. ^{1}H-MRS revealed a moderate reduction of NAA/Cr ratio in the left cerebellar hemisphere [0.90, -29% compared to mean n.v. = 1.27 (range: 0.91-1.75)], a sign of neuronal-axonal degeneration, while no CSF lactate was detected (data not shown).

As concerns Individual II-2 (Family 6), conventional brain MR sequences showed a mild cerebellar atrophy with hypoplastic optic nerves and chiasma, while ^{1}H-MRS metabolites' ratios in both VOIs were within the normal ranges. Diffusion images analysis demonstrated increased MD in the dentate nucleus (0.93 x 10-3mm2/s), pons (0.98 x 10-3mm2/s), superior cerebellar peduncles (1.03 x 10-3mm2/s) and cerebellar hemispheres (1.01 x 10-3mm2/s). Microstructural changes were milder compared to Family 6, Individual I-1.

Microsatellite genotyping at the *SIL1* [MIM 608005] locus, mutated in Marinesco-Sjogren syndrome [MIM 248800], did not reveal evidence of linkage with the disease. Therefore, the entire family quartet underwent WES, performed through target enrichment with the SeqCap EZ Human Exome Kit v2.0 by Roche Nimblegen (Roche Sequencing, Basel, Switzerland) and next-generation sequencing on an Illumina HiSeq2000 platform (Illumina, San Diego, CA, U.S.). The WES reads were aligned (reference human genome hg19) and processed as previously described,[5] obtaining mean depth of coverage (DoC) between 56.8X and 66.7X with 87.3-90.3% of targeted bases covered at >20X).

Assuming an autosomal recessive mode of inheritance, we examined homozygous or compound heterozygous coding variants (splice-sites, nonsynonymous changes and indels) with minor allele frequency (MAF) <0.01 or absent in public variant databases (1000 genomes, Exome Aggregate Consortium). WES confirmed the exclusion of *SIL1* mutations. No compound heterozygous variants of interest were identified. Homozygous variants were intersected with runs of homozygosity (ROH) longer than 500 kb detected by the H3M2 (Tanaka et al., 2015) software.[6] Previous SNP-array chip analysis on the four subjects using the ERSA software[7] revealed that the parents were likely 5th-degree relatives.

Detection of runs of homozygosity (ROHs) spanning several megabases in the two siblings is in line with the finding of moderately recent parental relatedness, further supporting implication of a variant inherited by descent. Only two homozygous variants, in *SAMD11* and *ATAD3A*, were identified in the same ROH of about 700 kb on distal chromosome 1p shared by the two siblings. Both variants were found to be in heterozygous state in the parents.

The homozygous *ATAD3A* variant (g.chr1:1447806C>T [hg19]; NM_001170535.1; c.158C>T; p.Thr53Ile) showed several features supporting its putative pathogenic role, including novelty, evolutionary conservation of the involved residue and high predicted pathogenicity score (**Table S3**). The *ATAD3A* variant and its segregation were confirmed by Sanger sequencing. Briefly, *ATAD3A* exon 1 was amplified from 20ng of siblings and parents' DNA by using KAPA2G Fast PCR Kit (Resnova) with 5% of dimethyl sulfoxide (DMSO) and 1.5 mM $MgCl_2$, with an annealing temperature of 60°C for 30 cycles. Forward and reverse primer sequences were 5'- AGA CTC TTC TCT GCG TCC TG -3' and 5'- AAA CCC ATC TAC CCA TCT GG -3', respectively. Sanger sequencing was performed through the BigDye

terminator v1.1 cycle sequencing kit (ThermoFisher Scientific) following the manufacturer's protocol.

Family 7, II-1

(Family 7, II-1 **(Figure 1A**) was a female born to a 35 yo G1P1 Indian mother and 32 yo Caucasian (western European ancestry) father at 34 5/7 wks, via emergent C-section for decreased fetal movement and breech position, and a nonreassuring nonstress test. The mother was treated for hypothyroidism during the pregnancy. Pregnancy was unremarkable until 32 wks, when mother noted some concern about decreased fetal movement. Fetal monitor demonstrated persistent minimal variability. C-section was undertaken at 34 5/7 due to the above, and the infant had low Apgar scores (2,4,8) and no respiratory effort, requiring intubation in the delivery room. Birthweight was recorded as 2130 grams, length 47.5 cm and head circumference 31 cm, with repeat measurements at 5 days as follows: weight 2110 grams, length 43.5 cm, HC 28.5 cm. Physical exam revealed bitemporal narrowing, short palpebral fissures, bilateral cloudy corneas but clear lenses, hypotonia and seizures. The infant had no spontaneous movement, and responded to painful stimulation by withdrawal of limbs. She was hypotonic with hypertonicity in distal hands and feet. She had bilateral clenched hands with flexion contractures of digits 3-5 and overlapping thumb and index finger. The thumb was straight and long, and she had bilateral rocker bottom feet deformities with curled in toes. Range of motion was decreased at the elbows and knees.

On day of life 2 she had episodes of jerking, and routine EEG after episodes showed long periods of discontinuity and epileptiform discharges with clinically

correlated seizures. Levetiracetam treatment was started. Head ultrasound revealed a large germinal hemorrhage, renal ultrasound was normal, and echo in the first days of life showed a large PDA, PFO, and mild right ventricular hypertrophy with septal hypertrophy. The proband had hypoglycemia after birth, hypernatremia, increased BUN, mild transaminitis and elevated triglycerides. Work-up included cell free DNA testing for aneuploidy during the 1st trimester of pregnancy which resulted normal. A fetal level II ultrasound at 17 weeks was normal. Infectious serologies were negative, and GBS status was unknown. Chromosome analysis after birth was normal, 46XX. Muscle biopsy showed nonspecific abnormalities, including increased fiber size variability, mildly increased internal nuclei, mildly increased myofiber lipid content/ droplet size, and probably type I fiber type predominance. COX staining did not reveal any abnormal mitochondria; however, these were not examined at higher resolution. CK was normal. Brain MRI demonstrated a smooth sulcal/gyral pattern, and significant hypoplasia of posterior fossa structures including cerebellum and brainstem.

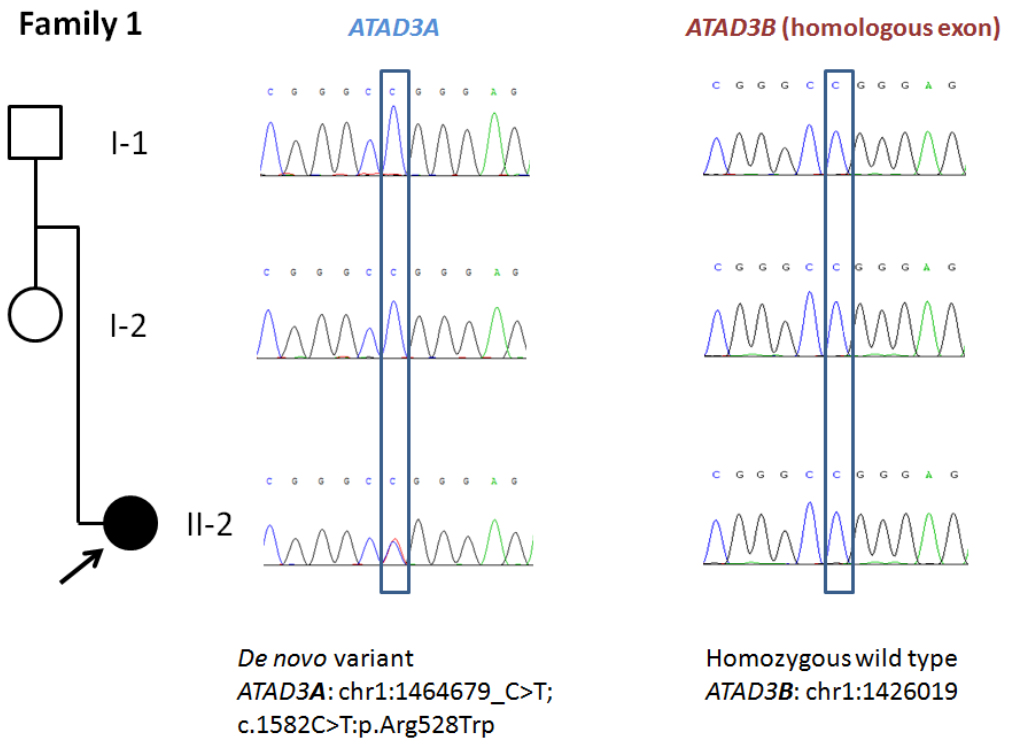

Figure S1. *ATAD3A* c.1582C>T variant is specific to *ATAD3A* and did not arise by gene conversion. Primer design utilizing specific intronic regions allowed for differentiation of the *ATAD3A* locus from the highly homologous *ATAD3B* locus. No variation was seen at the homologous *ATAD3B* locus, ruling out gene conversion as a mechanism of mutation. The paralogous exon in *ATAD3C* shares only 91.8% homology with this exon of *ATAD3A*, and is thus readily distinguishable. Additional single nucleotide variants (SNVs) would be expected to be seen if gene conversion occurred with *ATAD3C* as the donor paralog.

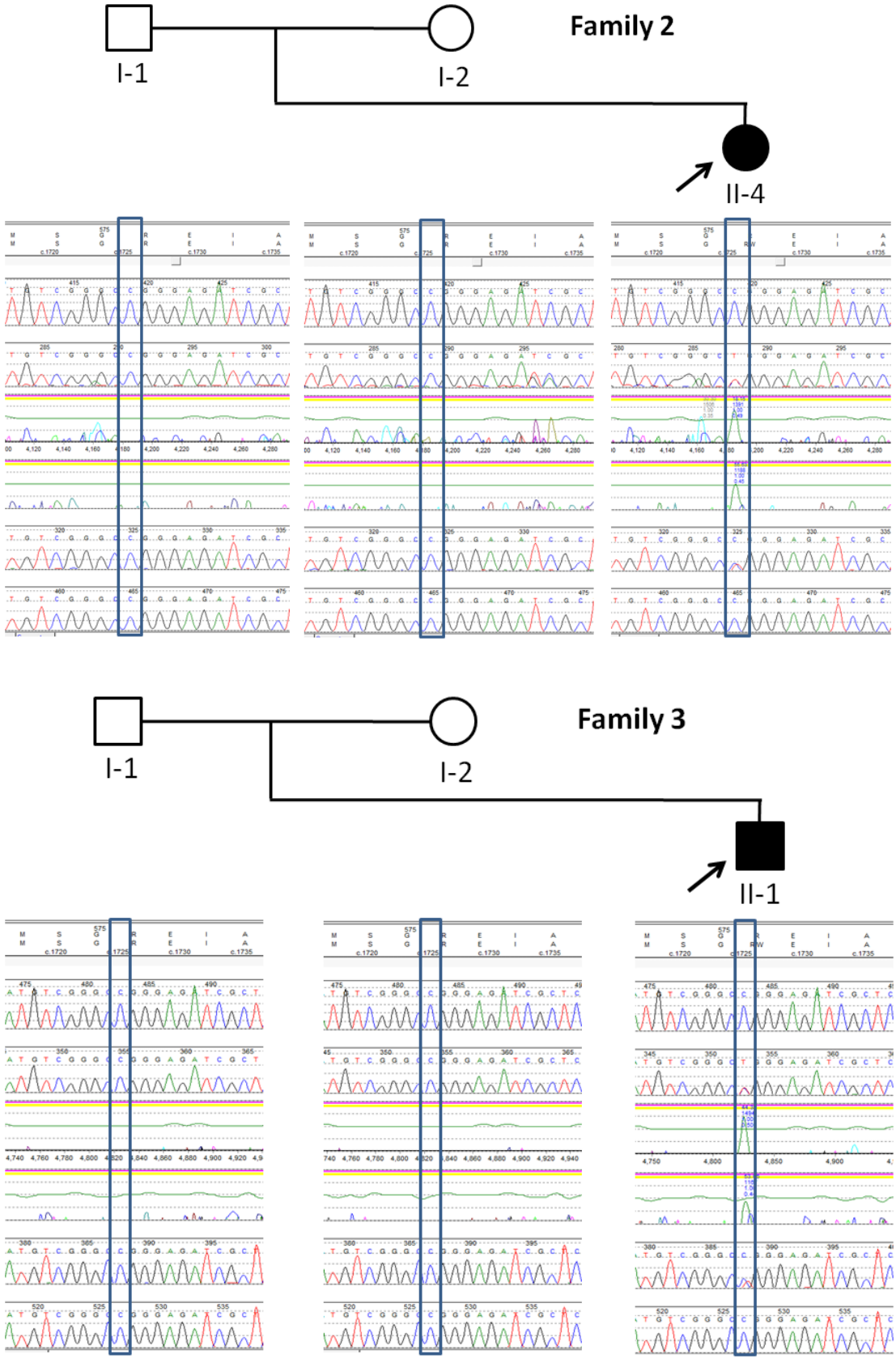

Figure S2. Sanger sequencing in Families 2 and 3 demonstrating the *de novo* c.1582C>T variant.

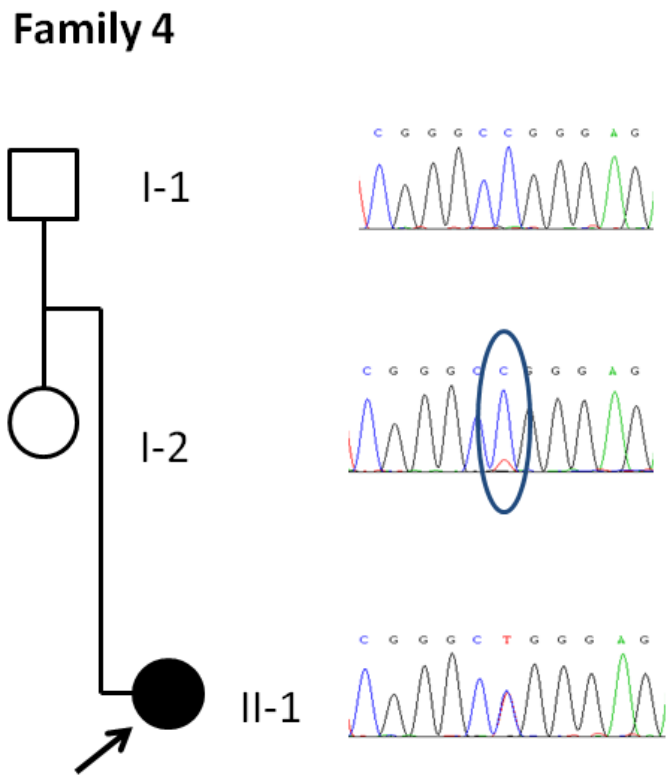

Figure S3. Sanger sequencing in Family 4 suggests low-level mosaicism in the mother.

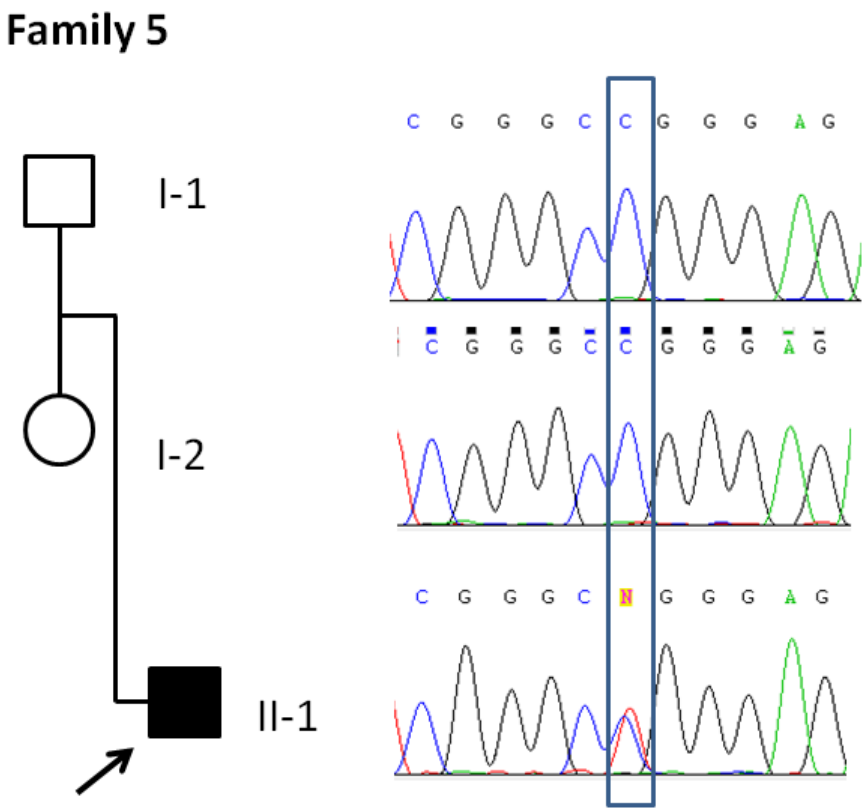

Figure S4. Sanger sequencing in Family 5 demonstrating the *de novo* c.1582C>T variant.

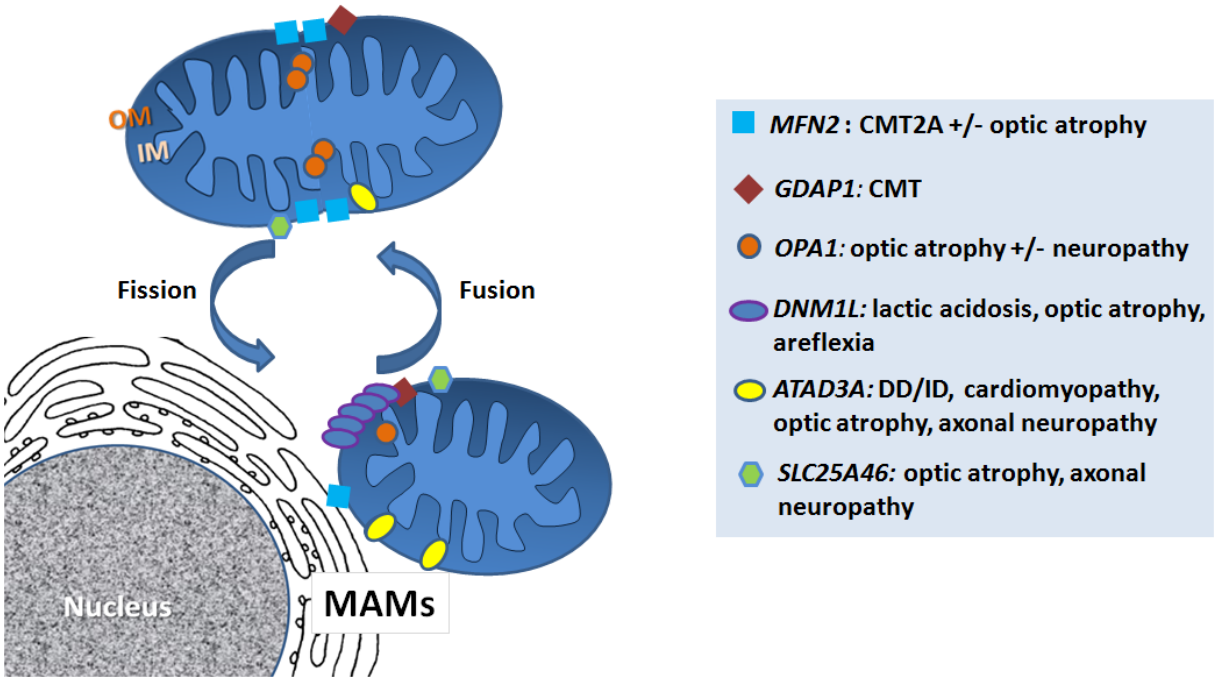

Figure S5. Fusion and fission proteins lead to neurological disease. Schematic diagram of select proteins involved in fusion and fission of mitochondria, and associated human disease.

abbreviations: OM – outer membrane; IM – inner membrane

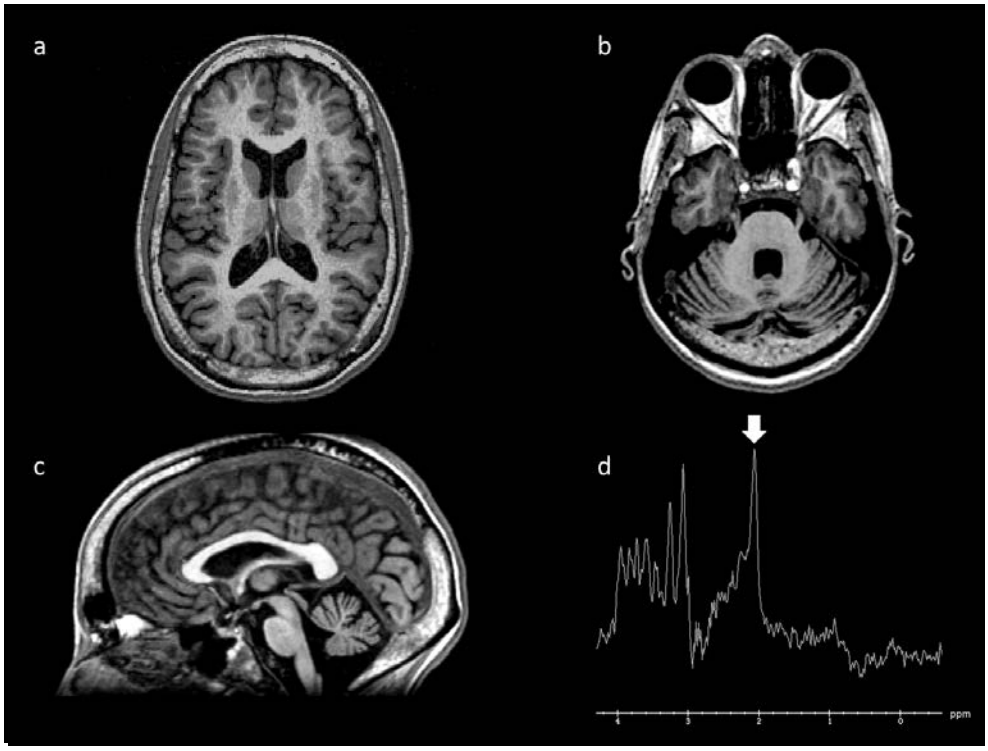

Figure S6. Brain imaging of Individual II-1 in Family 6.

Axial and sagittal brain high-resolution 3D T1 FSPGR images from Individual II-1 in Family 6. Images show an slight increase in the volume of the lateral and fourth ventricles, and atrophy of the cerebellar hemispheres and vermis. ^{1}H-MRS spectra from the left cerebellar hemisphere shows a reduction of the neuro-axonal marker N-Acetyl Aspartate content (arrow).

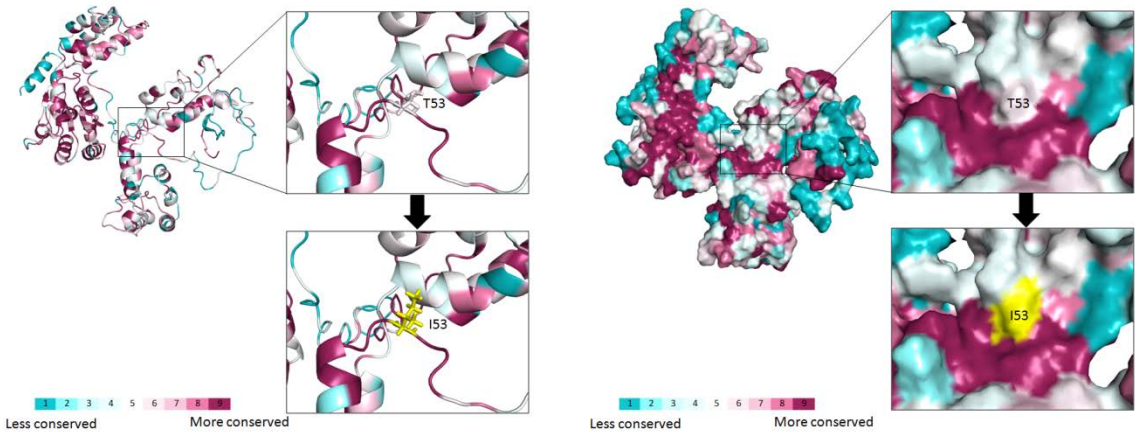

Figure S7. *In silico* modeling of p.Thr53Ile

Protein structure prediction shows that T53 is predicted to reside in coil and is solvent accessible (on the protein surface). The flanking amino acids 50-52 and 54-59 are highly conserved. Surface structure modeling (right) shows that T53 resides at the edge of a pocket, possibly a functional site, which consists of highly conserved residues. T53 may have a structural supporting role in this putative functional site, since T53 seems to protrude outward near the pocket.

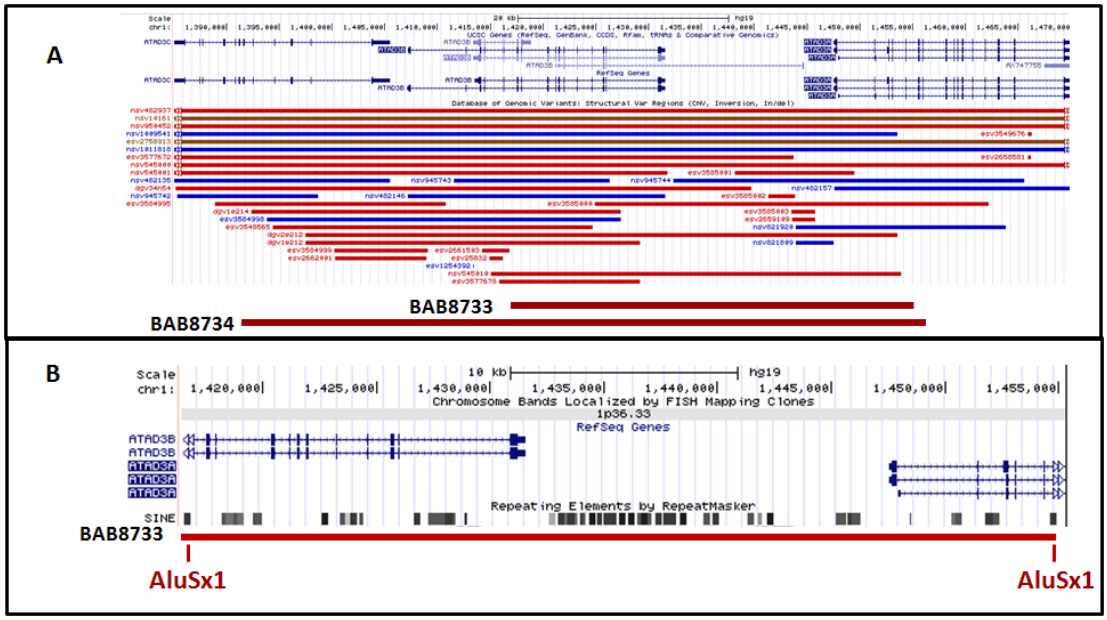

Figure S8. CNVs at the *ATAD3* locus. (A) Multiple CNVs have been reported in the *ATAD3* locus in the Database of Genomic Variants (DGV). Note rearrangements between paralogs. All tracks were derived from the UCSC genome browser. (B) The deletion breakpoints of BAB8733 include identical *Alu*Sx1 elements.

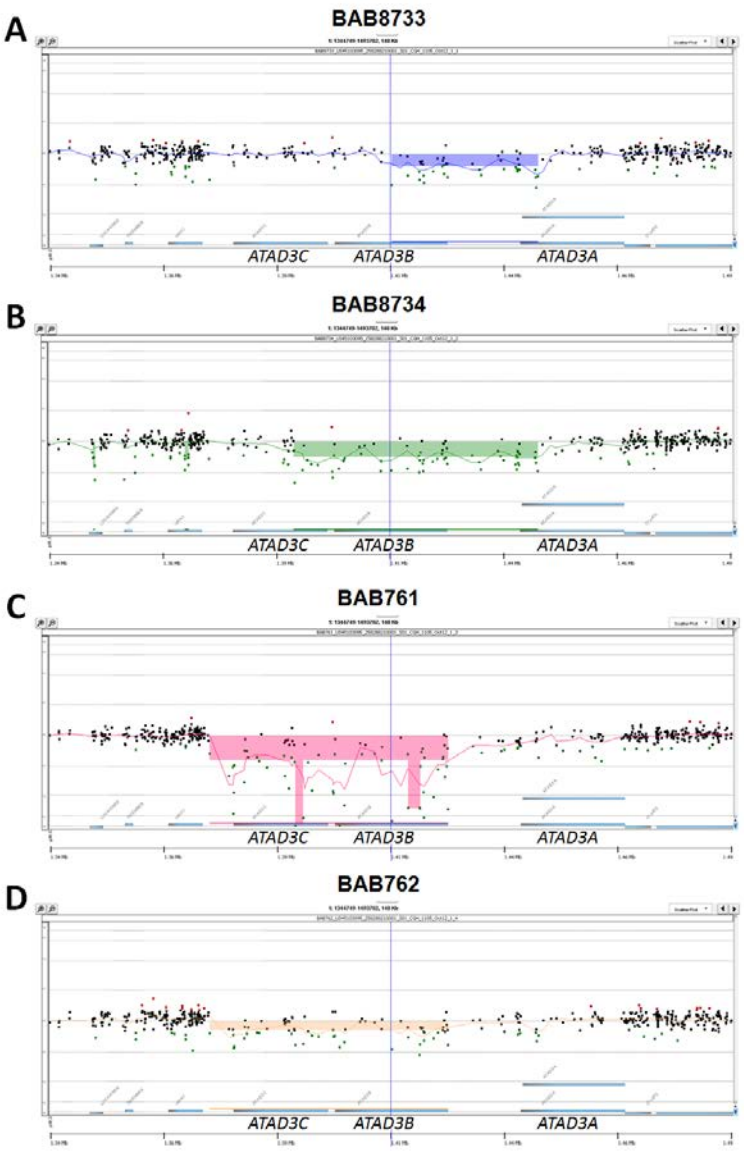

Figure S9. Targeted aCGH data. (A) Array of BAB8733 (Family 7, I-2) indicates a heterozygous deletion spanning from *ATAD3B* to *ATAD3A*. (B) Array of BAB8734 (Family 7, I-1) indicates a heterozygous deletion spanning from *ATAD3C* to *ATAD3A*. (C) Array of BAB761 indicates a homozygous deletion of *ATAD3C* and *ATAD3B*, without involvement of *ATAD3A*. (D) Array of BAB762 (mother of BAB761) indicates a heterozygous deletion of *ATAD3C* and *ATAD3B*.

A

```
CLUSTAL O(1.2.1) multiple sequence alignment

ATAD3B          tggattggtgttgagcatttttctggttttaaaggcttttctctttttctgcggcttctt 1416241
BAB8733         tggattggtgttgagcatttttctggttttaaaggcttttctctttttctgcggcttctt
ATAD3A          cccgcacacatgggcacagtcacaggttttaaaggcttttctctttttctgcggcttctt 1454295
                          * *      *  * ************************************

ATAD3B          ctcagCAACTTCTCAATGAGGAGAATTTACGGAAGCAGGAGGAGTCCGTGCAGAAGCAGG 1416301
BAB8733         ctcagCAACTTCTCAATGAGGAGAATTTACGGAAGCAGGAGGAGTCCGTGCAGAAGCAGG
ATAD3A          ctcagCAACTTCTCAATGAGGAGAATTTACGGAAGCAGGAGGAGTCCGTGCAGAAGCAGG 1454355
                ************************************************************

ATAD3B          AAGCCATGCGGCGAGgtaggctgtctgctctcctggctggggcggaggtggcgggggctg 1416361
BAB8733         AAGCCATGCGGCGAGgtaggctgtctgctctcctggctggggcggaggtggcgggggctg
ATAD3A          AAGCCATGCGGCGAGgtaggctgtctgctctcctggctggggcggaggtggcgggggctg 1454415
                ************************************************************

ATAD3B          cttgtggatccggcgtgcactctgagcctgagttctgccgcccggcccctcatagctacc 1416421
BAB8733         cttgtggatccggcgtgcactctgagcctgagttctgccgcccggcccctcatagctacc
ATAD3A          cttgtggacccggcgtgcactctgagcctgagttctgccgcccggcccctcatagctacc 1454475
                ******** ***************************************************

ATAD3B          agtgcagtgggcgaggcctgctggggctctgcggggtggggctcctctcggaagacacc 1416481
BAB8733         agtgcagtgggcgaggcctgctggggctctgcggggtggggctcctctcggaagacacc
ATAD3A          agtgcagtgggcgaggcctgctggggctccgcggggtggggctgcctctcggaagacacc 1454535
                *************************** ************* ****************

ATAD3B          tctgtctgcgagtggacgccaggatctgttcagggagggcaggagctgcttcacttcatg 1416541
BAB8733         tctgtctgcgagtggacgccaggatctgttcagggagggcaggagctgcttcacttcatg
ATAD3A          tctgtctgcgagtggacgccaggatctgttcagggagggcaggagctgcttcacttcatg 1454595
                ************************************************************

ATAD3B          ggaagtacaggggcctttttttttttttttgagacggagtctcgctctgtcacccaggcag 1416601
BAB8733         ggaagtacaggggcctttttttttttttttgagacggagtctcgctctgtcacccaggcag
ATAD3A          ggaagtacaggggcctttttttttttttttgagacggagtctcgctctgtcacccaggcag 1454655
                ************************************************************

ATAD3B          gagtgcaatagcacgatctcagctcactgcaacctctgcctcccaggtttaagcaattct 1416661
BAB8733         gagtgcaatagcacgatctcagctcactgcaacctctgcctcccaggtttaagcaattct
ATAD3A          gagtgcaatagcacgatctcagctcactgcaacctctgcctcccaggtttaagcaattct 1454715
                ************************************************************

ATAD3B          cctgcctcagcctcccgagtagctgggattataggctcccgccaccacgcccagctaatt 1416721
BAB8733         cctgcctcagcctcccgagtagctgggattataggctcccgccaccacgcccagctaatt
ATAD3A          cctgcctcagcctcccgagtagctgggattataggctcccgccaccacgcccagctaatt 1454775
                ************************************************************

ATAD3B          tttttgtatcttcagtagagaaagggtttcactgtgttggccaggctggtcttgaacttc 1416781
BAB8733         tttttgtatcttcagtagagaaagggtttcactgtgttggccaggctggtcttgaacttc
ATAD3A          tttttgtatcttcagtagagaaagggtttcactgtgttggccaggctggtcttgaacttc 1454835
                ************************************************************

ATAD3B          ttgatctcattatccgcctgccttggccttccacagtgctgggattacaggcgtgagcct 1416841
BAB8733         ttgatctcattatccgcctgccttggccttccacagtgctgggattacaggcgtgagcct
ATAD3A          ttgatctcattatccgcctgccttggccttccacagtgctgggattacaggcgtgagcct 1454895
                ************************************************************

ATAD3B          ctgcgttctgcctagaacatgggtctttactgtcctggtttcagtggggatcacaggtat 1416901
BAB8733         ctgcgttctgcctagaacatgggtctttactgtcctggtttcagtggggatcacaggtat
ATAD3A          ctgcgttctgcctagaacatgggtctttactgtcctggtttcagtggggatcacaggtat 1454955
                ************************************************************

ATAD3B          ttggtgccatgtggcatttgttggcgagtgctccaggcaaacgtctgtcaccactcttca 1416961
BAB8733         ttggtgccatgtggcatttgttggcgagtgctccaggcaaacgtctgtcaccactcttca
ATAD3A          ttggtgccatgtggcatttgttggcgagtgctccaggcaaacgtctgtcaccactcttca 1455015
                ************************************************************

ATAD3B          ccgtgggtgggcttgtggcgaggtgtgtgcgtttaatgttcagtagccaggcacgtggca 1417021
BAB8733         ccgtgggtgggcttgtggcgaggtgtgtgcgtttaatgttcagtagccaggcacgtggca
ATAD3A          ccgtgggtgggcttgtggcgaggtgtgtgcgtttaatgttcagtagccaggcacgtggca 1455075
                ************************************************************

ATAD3B          cgtcacgcgtgtctgagttctgacagctgtgtttctgtgtgaggggggcttccttcagaa 1417081
BAB8733         cgtcacgcgtgtctgagttctgacagctgtgtttctgtgtgaggggggcttccttcagaa
ATAD3A          cgtcacgcgtgtctgagttctgacagctgtgtttctgtgtgaggggggcttccttcagaa 1455135
                ************************************************************

ATAD3B          ctccgcgttctggtttttgcttcaaagagctcgtcctgagaagttgcctaggcctctgg 1417141
BAB8733         ctccgcgttctggtttttgcttcaaagagctcgtcctgagaagttgcctaggcctctgg
ATAD3A          ctccgcgttctggtttttgcttcaaagagctcgtcctgagaagttgcctaggcctctgg 1455195
                ************************************************************
```

```
ATAD3B          gtcggatttctgccctaatccatgggcagggccggcctgtggcgctgtccctaccaaggt 1417201
BAB8733         gtcggatttctgccctaatccatgggcagggccggcctgtggcgctgtccctaccaaggt
ATAD3A          gtcggatttctgccctaatccatgggcagggccggcctgtggcgctgtccctaccaaggt 1455255
                ************************************************************

ATAD3B          ctgtgtgtgtctgtggcacgggcctgtccatggactgggcttgtccgtggagtgggtcgg 1417261
BAB8733         ctgtgtgtgtctgtggcatggacctgtccgtggccttagcctattggcggcgtgggcctg
ATAD3A          ctgtgtgtgtctgtggcatggacctgtccgtggccttagcctattggcggcgtgggcctg 1455315
                ****************** ** ******* *** **  ** * *  * ** ***** * *

ATAD3B          tccatggccttagcctgttggtggcgtgggccggtccacggcatgggcctgtctgtggcg 1417321
BAB8733         tct-------------------------------------------------gtggcg
ATAD3A          tct-------------------------------------------------gtggcg 1455324
                **                                                  ******

ATAD3B          tgggccggtccgtggtgcgggcctgtccgtggccttagcctgttggtg 1417369
BAB8733         tgggcctgtccgtggccttagcctgtcagcagtgtgggcctgtccatg
ATAD3A          tgggcctgtccgtggccttagcctgtcagcagtgtgggcctgtccatg 1455372
                ****** ********     ******* *  *  *  ******   **
```

B

```
CLUSTAL O(1.2.1) multiple sequence alignment


ATAD3C          AAGGAACATCAAGAAGAACCGGGGCCTGTACAGGCACATCCTGCTGTACGGGCCACCAGG 1391271
BAB8734         AAGGAACATCAAGAAGAACCGGGGCCTGTACAGGCACATCCTGCTGTACGGGCCACCAGG
ATAD3A          AAGGAACACCAAGAAGAACCGCAGCCTGTACAGGAACATCCTGATGTACGGGCCACCAGG 1459319
                ******** ************ .***********.********.****************

ATAD3C          CACCGGGAAGACGCTGTTTGCCAAGgtgagagtgcctagctgaacaggtgggccaggggc 1391331
BAB8734         CACCGGGAAGACGCTGTTTGCCAAGgtgagagtgcctagctgaacaggtgggccaggggc
ATAD3A          CACCGGGAAGACGCTGTTTGCCAAGgtgagagcgcctggctgaacaggtgggccaggggc 1459379
                ******************************** ****.**********************

ATAD3C          cgctggggtctcacctgcctgcaggtgtctgggggggctcagctgcctggggaatggaccc 1391391
BAB8734         cgctggggtctcacctgcctgcaggtgtctgggggggctcagctgcctggggaatggaccc
ATAD3A          cgctggggtctcacctgcctgcaggtgtctgggggggctcagctgcctggggaatggaccc 1459439
                ************************************************************

ATAD3C          cccttaggcctttgcccaccctcgtgtaggctcagggtgctggtgtgggcagcagcgcct 1391451
BAB8734         cccttaggcctttgcccaccctcgtgtaggctcagggtgctggtgtgggcagcagcgcct
ATAD3A          cccttaggcctttgcccaccctcgtgtaggctcagggtgctggtgtgggcagcagcgcct 1459499
                ************************************************************

ATAD3C          cccatcttccaggcgggggacgtctcctgtctggcaggctgtggcttccaggcagggacg 1391511
BAB8734         cccatcttccaggcgggggacgtctcctgtctggcaggctgtggcttccaggcagggacg
ATAD3A          cccatcttccaggcgggggacgtctcctgtctggcaggctgtggcttccaggcagggacg 1459559
                ************************************************************

ATAD3C          ctgggcagagcctccacactccgggtggagtgtgcaggctttgcagaggcggagggaaca 1391571
BAB8734         ctgggcagagcctccacactccgggtggagtgtgcaggctttgcagaggcggagggaaca
ATAD3A          ctgggcagagcctccacactccgggtggagtgtgcaggctttgcagaggcggagggaaca 1459619
                ************************************************************

ATAD3C          tctgttctgtctcccctcactcttcttgtccagAAACTCGCCCTGCACTCAGGCATGGAC 1391631
BAB8734         tctgttctgtctcccctcactcttcttgtccagAAACTCGCCCTGCACTCAGGCATGGAC
ATAD3A          tctgctctgtctcccctcactcttcctgtccagAAACTCGCCCTGCACTCAGGCATGGAC 1459679
                **** ******************** ********************************

ATAD3C          TACGCCATCATGACAGGCGGGGACGTGGCCCCCATGGGGCGGGAAGGCGTGACCGCCATG 1391691
BAB8734         TACGCCATCATGACAGGCGGGGACGTGGCCCCCATGGGGCGGGAAGGCGTGACCGCCATG
ATAD3A          TACGCCATCATGACAGGCGGGGACGTGGCCCCCATGGGGCGGGAAGGCGTGACCGCCATG 1459739
                ************************************************************

ATAD3C          CACAAGCTCTTTGACTGGGCCAATACCAGCCGGCGCGGgtgagacgtccccacagcatgc 1391751
BAB8734         CACAAGCTCTTTGACTGGGCCAATACCAGCCGGCGCGGgtgagacgtccccacagcatgc
ATAD3A          CACAAGCTCTTTGACTGGGCCAATACCAGCCGGCGCGGgtgagacgtccccacagcatgc 1459799
                ************************************************************

ATAD3C          accaggcccttggctgcggcccagcaggctgccttctgggaaggggtccaggtgtctct 1391811
BAB8734         accaggcccttggctgcggcccagcaggctgccttctgggaaggggtccaggtgtctct
ATAD3A          accaggcccttggctgcggcccagcaggctgccttctgggaaggggtccaggtgtctct 1459859
                ************************************************************

ATAD3C          tggggaccctgtctttctgcagctctgtccttgtggccacgcaggaggcccagtggaggg 1391871
BAB8734         tggggaccctgtctttctgcagctctgtccttgtggccacgcaggaggcccagtggaggg
ATAD3A          tggggaccctgtctttctgcagctctgtccttgtggccacgcaggaggcccagtggaggg 1459919
                ************************************************************
```

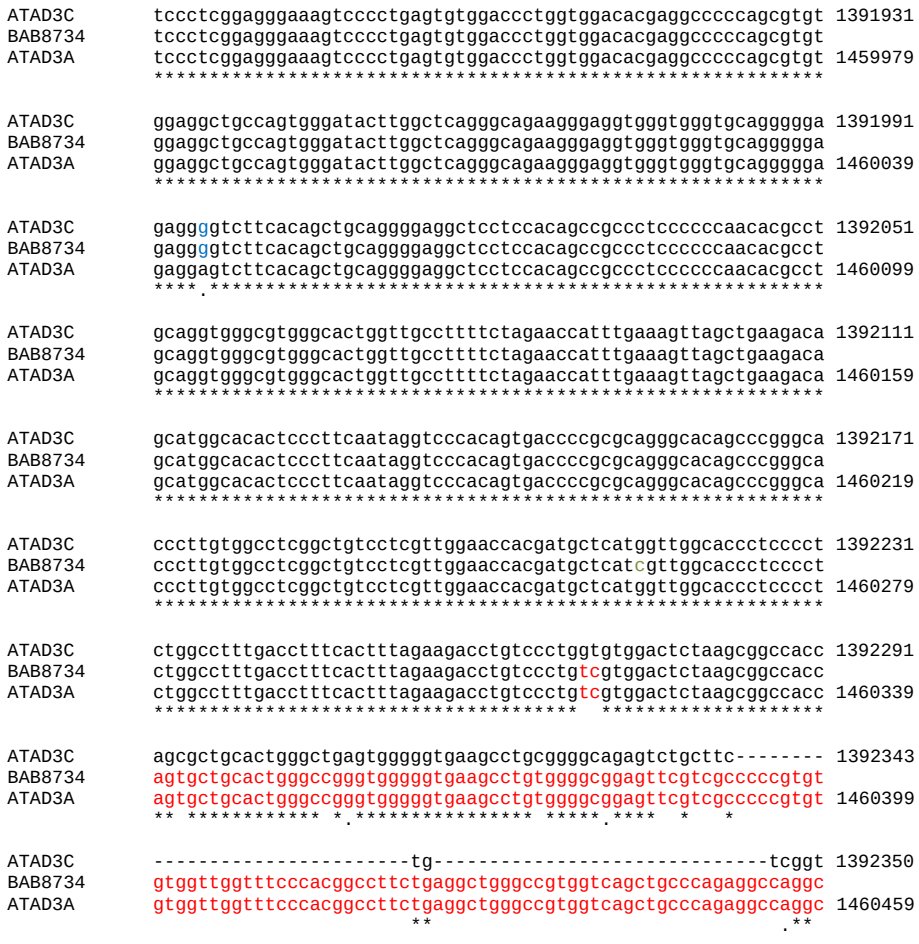

Figure S10. Breakpoint junction analyses in Family 7. (A) Nonallelic homologous recombination (NAHR) in BAB8733 (Family 7, I-2) is mediated by 754 bp of 100% homology in intron 5 of *ATAD3B* and *ATAD3A.* Blue font indicates sequence specific to *ATAD3B*, while red font indicates sequence specific to *ATAD3A. Alu*Sx1 element is shaded in grey. (B) NAHR in BAB8734 (Family 7, I-1) is mediated by 960 bp of 99.7% homology between the regions encompassing exon 7 of *ATAD3C* and exon 11 of *ATAD3A.*

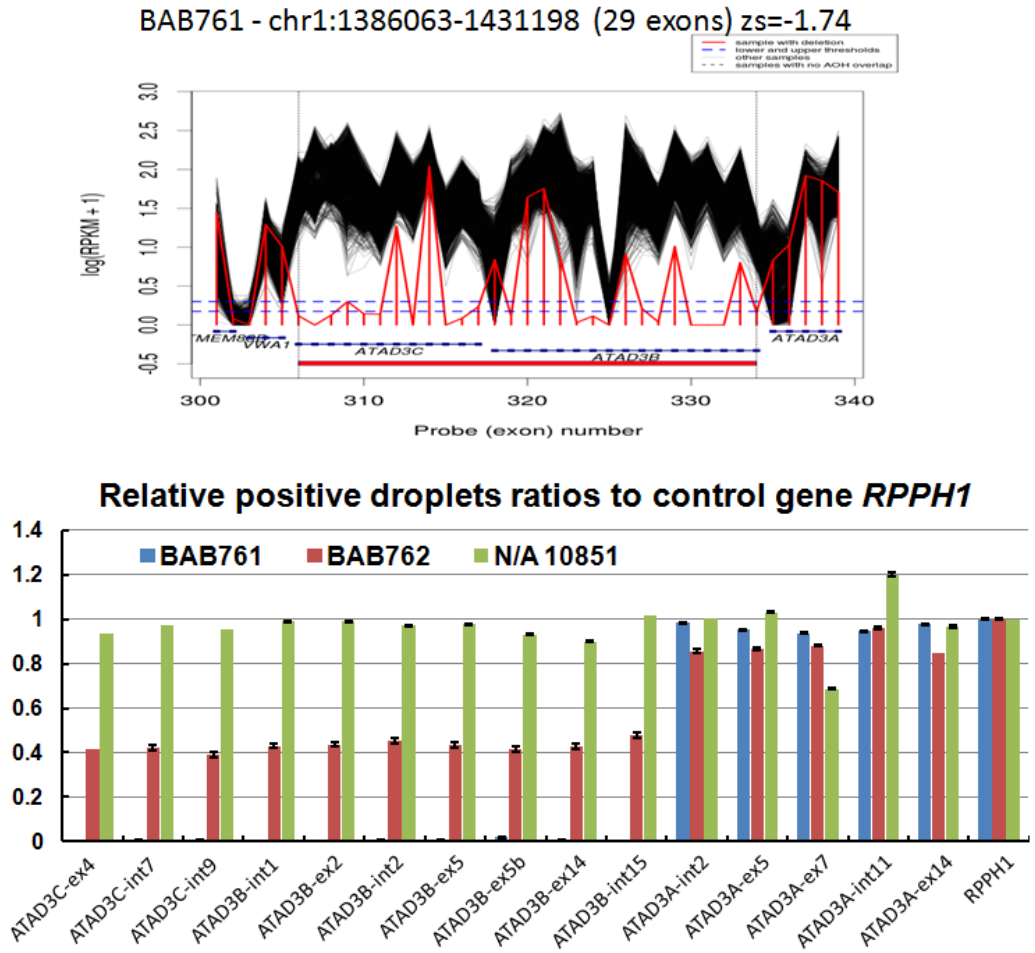

Figure S11. Homozygous CNV in BAB761 involving *ATAD3C* and *ATAD3B* narrows critical region to *ATAD3A*. Analysis of WES read depth in individual BAB761, with a clinical and molecular diagnosis of Smith Magenis syndrome, suggested a homozygous deletion of *ATAD3C* and *ATAD3B* (top). This was confirmed by droplet digital PCR (bottom). BAB761 showed no amplification of select exonic and intronic amplicons of *ATAD3C* and *ATAD3B*, and the proband's mother (BAB762) was heterozygous for these amplicons. Amplification of select *ATAD3A* exons and introns was comparable to controls.

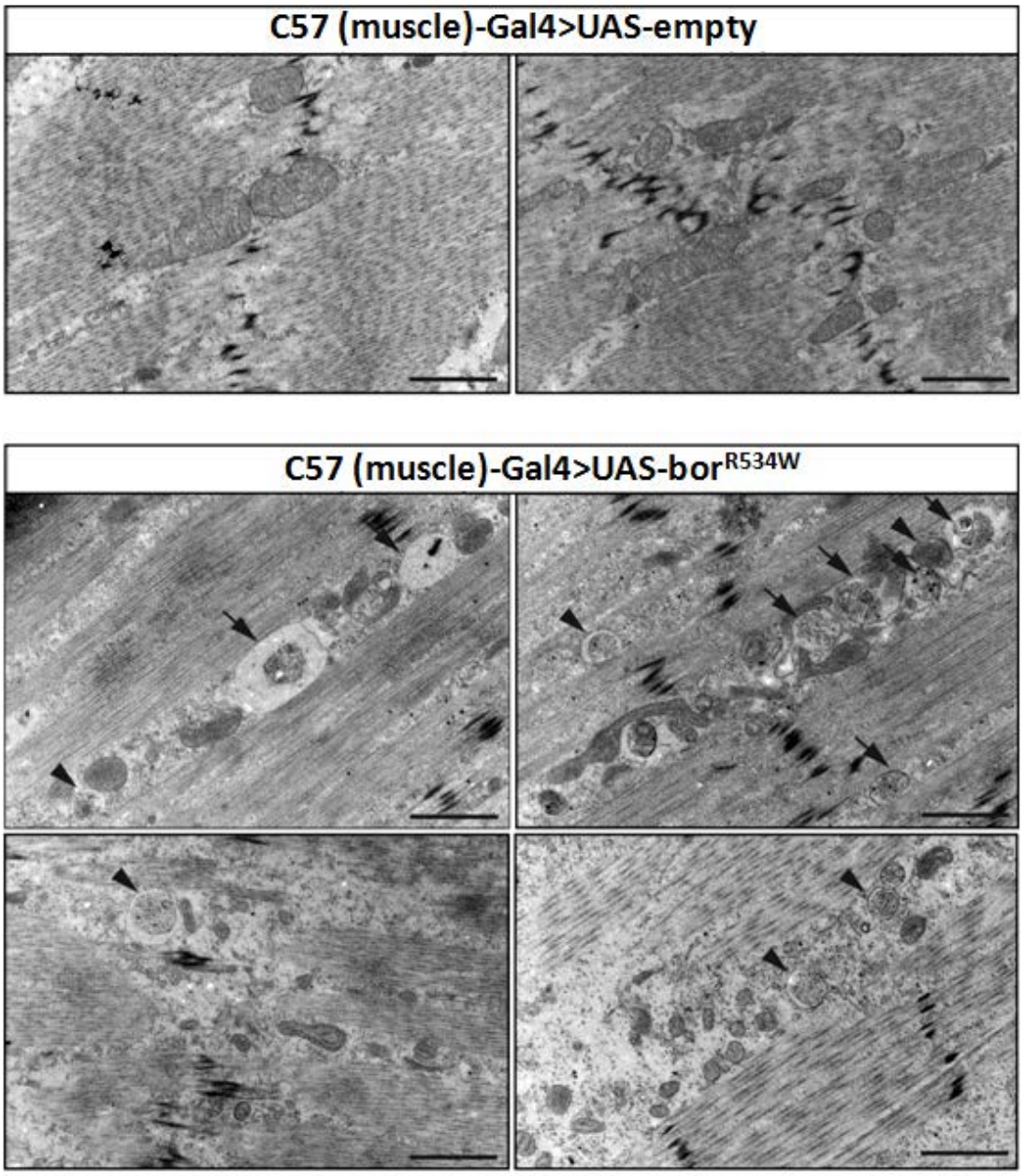

Figure S12. TEM sections of fly larvae muscle expressing *bor*^{R534W}

Top panels represent sections from fly larvae muscles carrying *C57 (muscle)-Gal4* together with *UAS*-empty (control) for comparison. Bottom panels represent sections from larvae muscles carrying *C57 (muscle)-Gal4* together with *UAS-bor*^{R534W}. Arrow heads indicate double-membraned autophagosomes. Arrows indicate autophagic vacuoles. Scale bar, 1 μm.

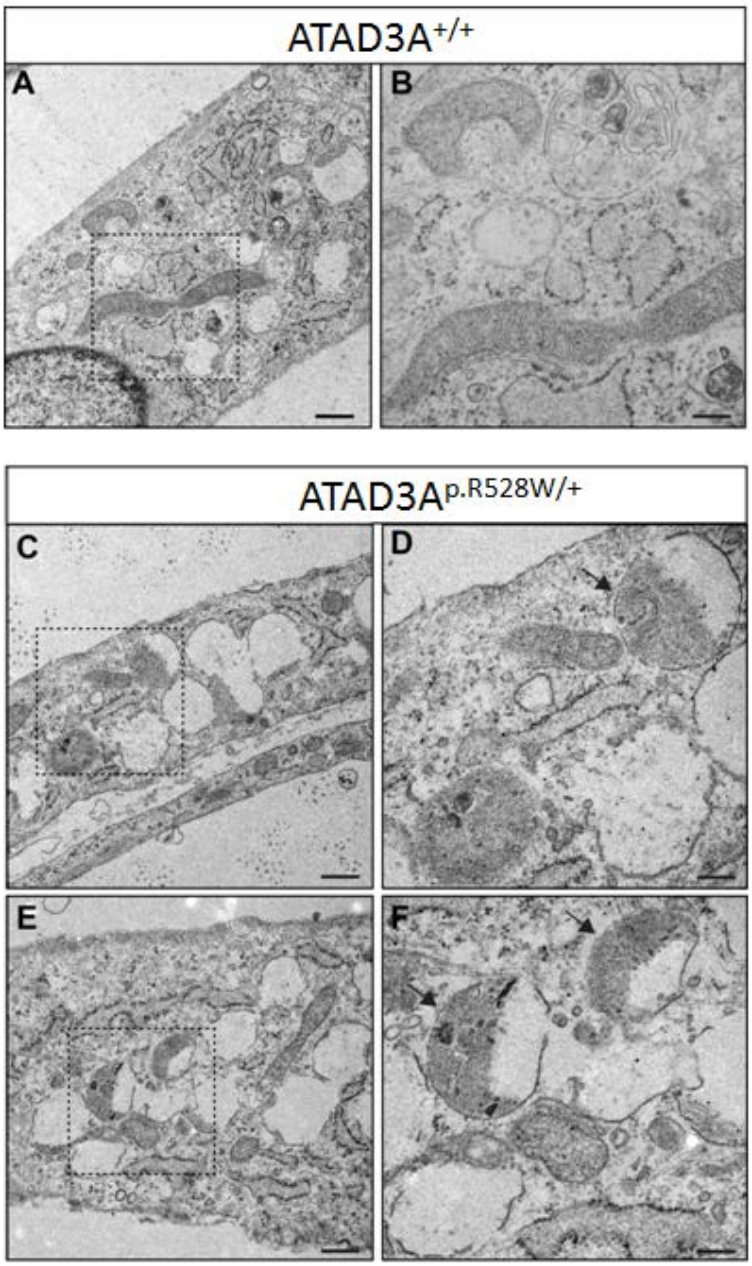

Figure S13. Fibroblasts from proband in Family 1 (*ATAD3A*$^{p.R528W/+}$) exhibit mitophagic events.

(A-B) TEM sections of control fibroblasts (*ATAD3A*$^{+/+}$). (C-F) TEM of fibroblasts from affected individual (Family 1, II-2, *ATAD3A*$^{p.R528W/+}$). (B), (D), and (F) are high magnification images of inserts in (A), (C), and (E), respectively. Arrows indicate mitophagic vesicles. (A,C,E) Scale bars 500 nm. (B,D,F) Scale bars 200 nm.

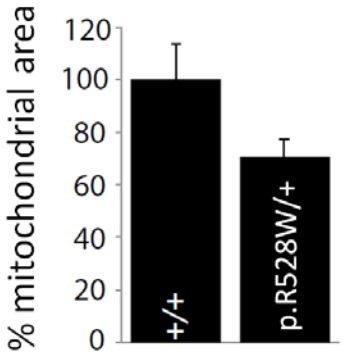

Figure S14. Mitochondria are reduced in fibroblasts from Family 1, II-2.

Percentage of area of mitochondria divided by area of cell in affected (*ATAD3A*$^{p.R528W/+}$) and control (*ATAD3A*$^{+/+}$) fibroblasts. Error bars indicate s.e.m. P values were calculated using Student's t-test. P=0.067

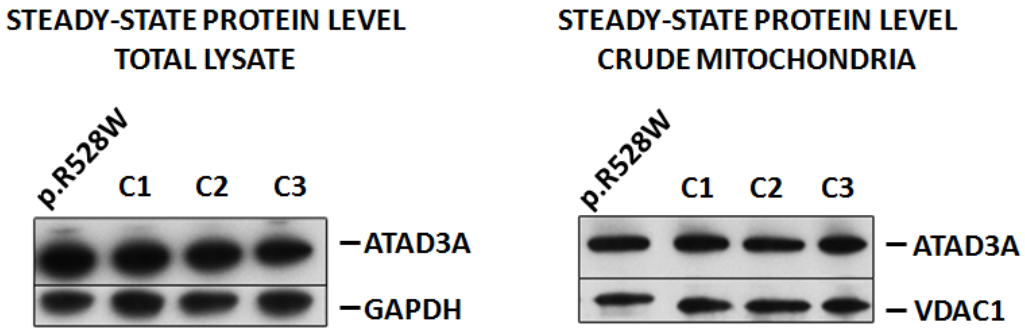

Figure S15. Steady-state levels of ATAD3A protein in fibroblasts.

Western blot analysis of steady-state levels of ATAD3A protein in total lysate (left) and crude mitochondria (right) in the proband from Family 4. Protein levels are not reduced in fibroblasts carrying the p.R528W mutation. Abbreviations: C1 - control 1, C2 - control 2, C3 - control 3.

Table S2. Primer locations and results of droplet digital PCR (ddPCR).

Gene	Forward primer start [chr1:hg19]	Reverse primer end [chr1:hg19]	ddPCR result mother (concentration)	ddPCR result father (concentration)	ddPCR result control (concentration)	ddPCR result mother (# alleles)	ddPCR result father (# alleles)
ATAD3C	1389781	1389985	278	308	278	2	2
ATAD3C	1392335	1392489	292	148	281	2	1
ATAD3C	1395761	1395980	275	146	275	2	1
ATAD3B	1409276	1409458	290	156	290	2	1
ATAD3B	1412616	1412791	288	150	293	2	1
ATAD3B	1413765	1413934	305	158	236	2	1
ATAD3B	1416142	1416386	288	153	250	2	1
ATAD3B	1425606	1425810	157	154	268	1	1
ATAD3B	1426134	1426358	149	146	224	1	1
ATAD3A	1452433	1452604	151	151	270	1	1
ATAD3A	1454246	1454438	146	151	251	1	1
ATAD3A	1455969	1456171	272	149	286	2	1
ATAD3A	1460392	1460617	295	330	344	2	2
ATAD3A	1462949	1463118	273	297	281	2	2
RPPH1	chr14:20811230	chr14:20811309	298	306	296	2	2

Table S3. *ATAD3A* variants, frequency and bioinformatic predictions (NM_001170535.1)

Gene	Chromosome position	Sequence alteration	Protein alteration	Zygosity	ExAC frequency	CADD score	Phylop	SIFT	Mutation taster
ATAD3A	Chr1: 1464679 C>T	c.1582C>T	p.Arg528Trp	Het	0	27.6	1.207	0	0.9999
ATAD3A	Chr1: 1447806 C>T	c.158C>T	p.Thr53Ile	Hom	0	34	4.956	0	0.9999

Table S4. Mitochondrial respiratory chain enzyme analysis in muscle homogenate and in skin fibroblasts

	Muscle						***Fibroblasts***					
	CI	**CII**	**CIII**	**CIV**	**SDH**	**CS**	**CI**	**CII**	**CII**	**CIV**	**SDH**	**CS**
Family 6, II-2	23.1	41.2	210	250	25.1	136	16.7	16.8	134	121	12.1	166
Family 6, II-1	n.a.	n.a.	n.a.	n.a.	n.a.	n.a.	18.2	19.9	139	134	16.8	133
mean ± sd	25,2 ± 4,4	19,9 ± 4,4	100 ± 15	189 ± 33	13,6 ± 2,6	133 ± 39	23,7 ± 4,6	19,2 ± 3,4	119 ± 15	150 ± 30	13,6 ± 2,7	113 ± 18
range	16,6 – 33.8	11,4 - 28,4	70 - 130	124 - 253	8,5 - 18,7	56 - 209	14,7 - 32,7	12,5 - 26,0	90 - 148	91 - 209	8,3 - 18,8	78 - 149
(m ± sd)												
	Muscle						***Fibroblasts***					
Family 4, II-1	-	-	-	-	-	-	20.07	13.13	19.28	33.08	8.52	61.17
mean ± sd	-	-	-	-	-	-	15.66 ±5.5	11.51 ±1.45	20.83 ±4.62	35.56 ±5.83	7.79 ±2.34	64.29 ±31.6

1. Tanaka, A. J., Cho, M. T., Millan, F., Juusola, J., Retterer, K., Joshi, C., Niyazov, D., Garnica, A., Gratz, E., Deardorff, M., et al. (2015). Mutations in SPATA5 Are Associated with Microcephaly, Intellectual Disability, Seizures, and Hearing Loss. Am. J. Hum. Genet. *97*, 457-464.

2. Lodi, R., Parchi, P., Tonon, C., Manners, D., Capellari, S., Strammiello, R., Rinaldi, R., Testa, C., Malucelli, E., Mostacci, B., et al. (2009). Magnetic resonance diagnostic markers in clinically sporadic prion disease: a combined brain magnetic resonance imaging and spectroscopy study. Brain *132*, 2669-2679.

3. Provencher, S.W. (1993). Estimation of metabolite concentrations from localized in vivo proton NMR spectra. Magn. Reson. Med. *30*, 672-679.

4. Provencher, S.W. (2001). Automatic quantitation of localized in vivo 1H spectra with LCModel. NMR Biomed. *14*, 260-264 (2001).

5. Bonora, E., Bianco, F., Cordeddu, L., Bamshad, M., Francescatto, L., Dowless, D., Stanghellini, V., Cogliandro, R. F., Lindberg, G., Mungan, Z., et al. (2015). Mutations in RAD21 disrupt regulation of APOB in patients with chronic intestinal pseudo-obstruction. Gastroenterology *148*, 771-782.

6. Magi, A., Tattini, L., Palombo, F., Benelli, M., Gialluisi, A., Giusti, B., Abbate, R., Seri, M., Gensini, G. F., Romeo, G. et al. (2014). H3M2: detection of runs of homozygosity from whole-exome sequencing data. Bioinformatics *30*, 2852-2859.

7. Huff, C. D., Witherspoon, D. J., Simonson, T. S., Xing, J., Watkins, W. S., Zhang, Y., Tuohy, T. M., Neklason, D. W., Burt, R. W., Guthery, S. L., et al. (2011). Maximum-likelihood estimation of recent shared ancestry (ERSA). Genome Res. *21*, 768-774.